

# Adnexal Masses: Characterization of Benign Ovarian Lesions

ROSEMARIE FORSTNER and KAREN KINKEL

## CONTENTS

9.1	<b>Introduction</b>	197
9.2	<b>Technical Recommendations for Ovarian Lesion Characterization</b>	197
9.3	<b>Defining the Origin of a Pelvic Mass: Adnexal Versus Extra-adnexal Versus Extraperitoneal</b>	199
9.4	<b>Characterizing Ovarian Lesions</b>	202
9.4.1	Differentiation Between Benign and Malignant Ovarian Lesions	202
9.4.2	Functioning Ovarian Tumors	207
9.4.2.1	Value of Imaging	209
9.4.3	Ovarian Tumors in Children, Adolescents, and Young Women	209
9.4.3.1	Value of Imaging	211
9.4.4	Adnexal Masses in Pregnancy	211
9.4.4.1	Value of Imaging	210
9.5	<b>Benign Adnexal Lesions</b>	212
9.5.1	Non-neoplastic Lesions of the Ovaries and Adnexa	212
9.5.1.1	Physiologic Ovarian Cysts	212
9.5.1.2	Paraovarian Cysts	214
9.5.1.3	Peritoneal Inclusion Cysts	215
9.5.1.4	Theca Lutein Cysts	216
9.5.1.5	Polycystic Ovary Syndrome	216
9.5.2	Benign Neoplastic Lesions of the Ovaries	219
9.5.2.1	Cystadenoma	219
9.5.2.2	Cystadenofibroma	221
9.5.2.3	Benign Teratoma	221
9.5.2.4	Benign Sex Cord Stromal Tumors	225
	<b>References</b>	229

R. FORSTNER, MD  
 PD, Department of Radiology, Landeskliniken Salzburg,  
 Paracelsus Private Medical University, Müllner Hauptstrasse  
 48, 5020 Salzburg, Austria  
 K. KINKEL, MD, PD  
 Institut de Radiologie, Clinique des Grangettes, chemin des  
 Grangettes 7, 1224 Chêne-Bougeries, Switzerland

## 9.1

### Introduction

Thorough pretreatment assessment by cross-sectional imaging plays a pivotal role in the management of suspected adnexal masses. It guides the surgeon to anticipate malignancy before starting surgery and aids in planning the adequate therapeutic approach. In this context, in benign ovarian lesions laparoscopy has been widely replacing open surgery. This is why pretreatment knowledge of imaging findings in various ovarian lesions is of utmost importance. Although a definite histopathologic diagnosis is not possible in the majority of cases, predicting the likelihood of malignancy is crucial for proper patient management [1].

In the assessment of adnexal masses the following parameters should be addressed by imaging: (a) defining the exact origin of the mass, (b) if the lesion is ovarian to define if it is a physiologic or neoplastic finding, and (c) when surgery is warranted for a neoplastic lesion, imaging findings concerning the risk of malignancy may assist the surgeon in deciding between laparoscopy or laparotomy [2].

## 9.2

### Technical Recommendations for Ovarian Lesion Characterization

MRI of the female pelvis is performed after 5 h of fasting and with prior intramuscular injection of peristaltic inhibitors to minimize artifacts due to bowel movement. The patient lies on her back in a supine position with a pelvic, torso, or cardiac coil attached around her pelvis. The coil ideally covers the region from the symphysis pubis up to the renal hilum. Depending on the woman's height, upper coverage may be lower and require secondary adjustment of the

coil if hydronephrosis or retroperitoneal lymphadenopathy is suspected.

Ovarian cyst characterization requires good anatomical coverage of the entire ovarian cyst and the uterus to be able to confirm the ovarian vs uterine origin of the mass.

The imaging protocol implies the use of both T2- and T1-weighted sequences. High-resolution fast spin echo T2-weighted images are mandatory to confirm the anatomical origin and clearly identify the ovarian nature of the mass. Further tissue characterization takes into account signal intensity at three subsequent T1-weighted sequences in the following order: native, fat-suppressed, and after intravenous injection of gadolinium. The latter contrast-enhanced sequence is mandatory to exclude malignancy. Identical slice orientation allows exact comparison of all T1-weighted sequences. Table 9.1 demonstrates differences in signal intensity according to the histological type of the most frequent ovarian neoplasm.

**Table 9.1.** Signal intensity of benign ovarian masses on MRI of the pelvis according to sequences and histological lesion type

Histology of ovarian neoplasm	Signal intensity		
	T2	Native T1	Fat-suppressed T1
Serous cystadenoma	High	Low	Low
Mucinous cystadenoma	High	Intermediate	Intermediate
Mature cystic teratoma	Intermediate	High	Low
Endometrioma	High	High	High
Fibroma	Low-intermediate	Intermediate	Intermediate

Turbo spin echo (TSE) sequences are the sequences of choice due to their excellent image resolution. Imaging parameters include a field of view of 200–300 mm with a matrix of 512×256, slice thickness between 4 and 5 mm, and a number of signal acquisitions between two and four. T2-weighted fast spin echo (FSE) sequences use a TR/TE around 4,000/90 ms, whereas the TR for T1-weighted sequences is around 500 ms with a minimum TE. Due to time restrictions, faster T2-weighted sequences such as ultrafast half-Fourier single-shot turbo spin-echo sequences (HASTE, 3 s per slice) have been tested in 60 female pelvis ex-

aminations and compared to conventional and high-resolution turbo spin echo sequences [3]. A HASTE sequence is applied with a TR/effective TE/echo train of infinity/90/64 and a 128×256 matrix. HASTE provided clearer visualization of large leiomyomas and ovarian tumors but slightly poorer visualization of uterine cancer compared to high-resolution turbo spin echo sequences. One of the advantages was greater time efficacy without motion and chemical shift artifacts. Lesion conspicuity was better with HASTE than with conventional TSE imaging (matrix, 128×256) but lower than with high-resolution TSE (matrix, 300×512). Because of limited image resolution, the HASTE sequence should be used when the high-resolution TSE imaging is suboptimal or to provide additional imaging planes as a complement to high-resolution TSE. T2-weighted echo planar sequences (EPI) were not successful in the female pelvis compared to fast spin echo sequences. The study showed inferior uterine zonal anatomy and ovarian visualization in 44 (56%) of 78 and 18 (33%) of 54 cases, respectively [4]. Ovarian cystic lesions were revealed more precisely by the fast spin-echo sequence than by the EPI sequence. When T1-weighted sequences were compared in a pelvic and abdominal MRI study including 70 patients, the EPI T1 sequence allowed a 40% reduction in acquisition time without difference in the diagnostic performance of three reviewers [5].

To allow the distinction of an ovarian vs uterine origin of a mass, dynamic contrast injection might be helpful to better delineate the early enhancing normal myometrium [6]. This type of sequence is acquired once before and three times after IV contrast injection and corresponds to a 2D TSE sequence with 18 slices of 4 mm at a FOV of 300 mm, a matrix of 202×512, a TSE factor of 5, a TR/TE of 550/14 with two numbers of signal acquisition and a total acquisition time of 6 min.

For ovarian lesion characterization, intravenous contrast injection has been shown to be mandatory because of its ability to identify solid intracystic portions such as papillary projections, necrosis within a solid mass, septation or wall thickening Fig. 9.1 [7]. The multivariate logistic regression analysis also demonstrated different predictive values to identify malignancy according to the MRI signs. The highest odds ratio for malignancy was found for “necrosis in a solid lesion,” with an odds ratio of 107, followed by the sign “vegetation in a cyst” with an odds ratio of 40. Identification of enhancement within a T1-hyperintense cyst might require a subtraction technique

(contrast-enhanced fat-suppressed T1-weighted sequence minus native fat-suppressed T1-weighted sequence) to demonstrate the enhancing solid portion within a hyperintense endometrioma. This sign has recently been reported to be highly suggestive of associated ovarian carcinoma [8]. Careful inspection and comparison of T2- and T1-weighted images help identify this possibility. The number of T2-weighted acquisitions depends on imaging time but should cover at least two orthogonal imaging planes and ideally represent all three imaging planes to allow the choice of the best anatomical slice orientation for the three T1-weighted sequences.

Because of its inferior soft tissue contrast compared to MRI, CT is not the imaging modality of choice for further characterization of adnexal lesions detected at sonography. In contrast, for staging of suspected ovarian cancer it remains the primary imaging modality. Other indications for CT include contraindications for MRI, assessment of acute pelvic pain and to rule out complications of pelvic inflammatory disease. Due to its wide clinical use, however, many adnexal lesions are encountered by CT examinations. The use of bowel opacification is generally recommended in the assessment of adnexal lesions. It is crucial in the differentiation of fluid filled-bowel and cystic adnexal lesions and improves the identification of peritoneal seeding. Furthermore, especially in thin patients and in postmenopausal age, detection of normal ovaries is often only possible with bowel opacification. For this purpose, 1,000 ml of diluted contrast media or alternatively water are administered 1 h prior to the CT study. Rectal opacification is also helpful, especially if the oral contrast was not given early enough. Intravenous contrast opacification is pivotal for assessing adnexal lesions. It allows better characterization of the internal architecture and differentiation of pelvic vascular structures, including depiction of the ovarian vascular pedicle. In most cases, a venous phase enables best depiction of intralésional structures, as solid enhancing components and papillary projections may be missed in an early phase. A dual phase protocol, however, consisting of an arterial and venous phase may aid in improved assessment of the local extent or the anatomical relationships of an adnexal lesion. If a dermoid is suspected sonographically, a study without i.v. contrast media may be sufficient. However, torsion can only be assessed after contrast media application. In cases of large endometriomas a noncontrast study may also be helpful to differentiate hemorrhage from enhancing solid areas.

### 9.3

#### **Defining the Origin of a Pelvic Mass: Adnexal Versus Extra-adnexal Versus Extraperitoneal**

Defining the correct origin is the first diagnostic step in defining treatment of a suspected adnexal mass. Depending on the site of origin the differential diagnoses and treatment options often differ completely. Size, architecture, and location may appear similar in adnexal, extra-adnexal peritoneal masses, and even extraperitoneal lesions. However, special features determining the anatomical relationship of the mass and the surrounding pelvic anatomical structures can assist in their differentiation [9]. These parameters include visualization of ovarian structures, the type of contour deformity at the interface between the ovary and the pelvic mass, and the displacement pattern of the vessels, ureters, and other pelvic organs.

Identifying a mass separate from the ipsilateral ovary indicates its nonovarian origin (Fig. 9.2). However, especially in large pelvic lesions, the ovary may often be obscured or totally invaded by the mass [10]. Especially in smaller lesions when the ovary is not completely obscured, identifying ovarian structures, usually ovarian follicles, indicate its ovarian origin (Fig. 9.3). Furthermore, for this purpose analyzing specific signs such as the beak sign, and the embedded organ sign can aid in better defining its relationship with the ovary. When a mass deforms the edge of the ovary into a beak shape it is likely that it arises from the ovary (Fig. 9.3). In contrast, dull edges at the interface with the adjacent ovary suggest that the tumor compresses the ovary but does not arise from it [9].

Large ovarian masses typically displace the ureter posteriorly or posterolaterally. The same displacement pattern, however, can be caused by other intraperitoneal lesions, such as the bladder, and masses arising from the uterus or bowel [11]. The iliac vessels are typically displaced laterally by an adnexal lesion. In contrast, medial displacement of the iliac vessels is typical for extraovarian masses, originating from the pelvic wall or in lymphadenopathy (Fig. 9.4). The origin of a mass may be further elucidated by tracking the vascular pedicle or the ovarian suspensory ligament [9]. The presence of ovarian vessels leading to or emerging from an adnexal mass was identified in 92% of ovarian lesions on helical CT [12]. Defining the ovarian vascular pedicle allows the differentiation from lesions mim-

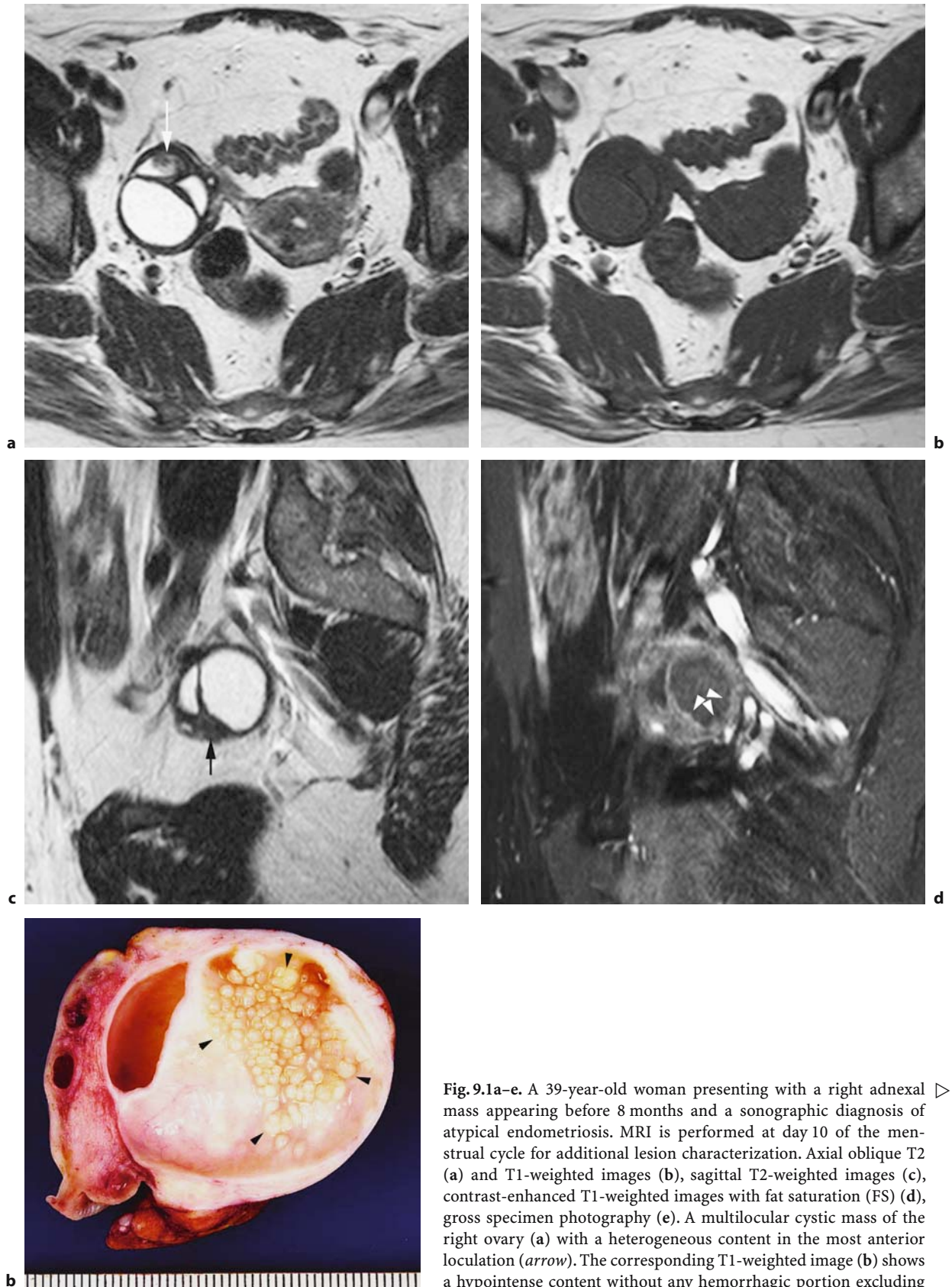
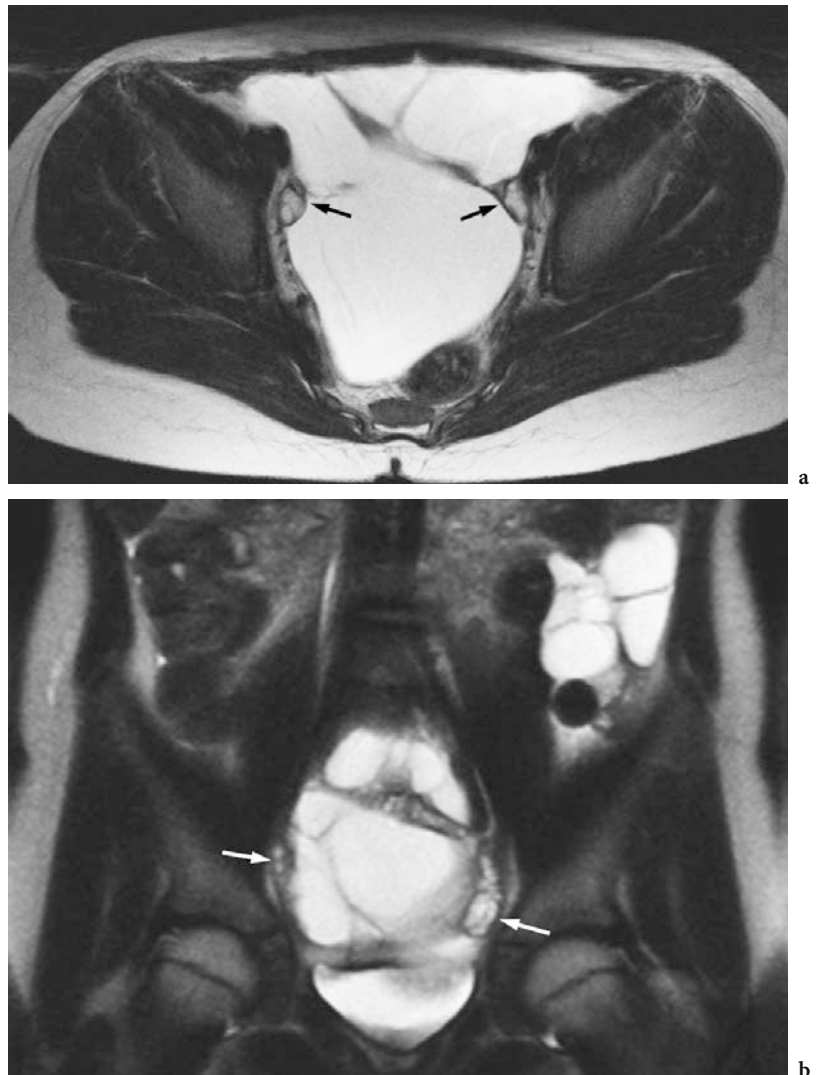
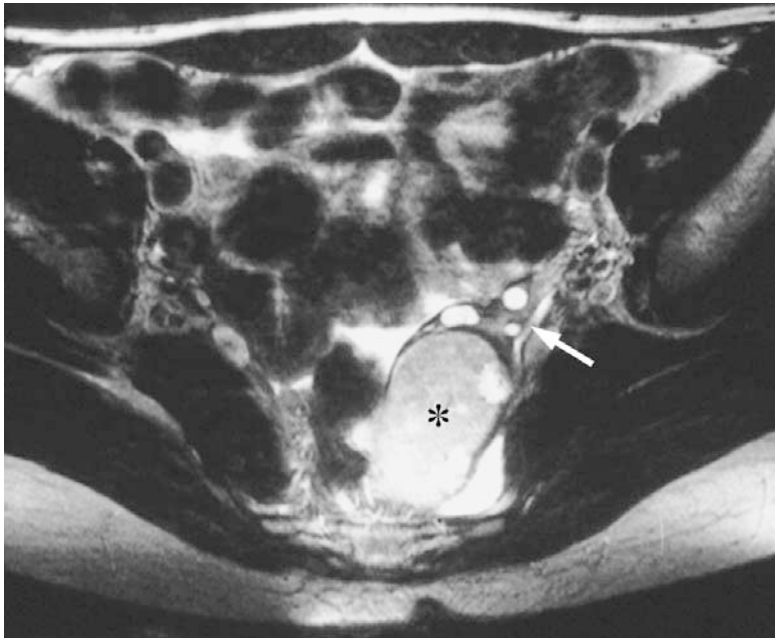


Fig. 9.1a-e. A 39-year-old woman presenting with a right adnexal mass appearing before 8 months and a sonographic diagnosis of atypical endometriosis. MRI is performed at day 10 of the menstrual cycle for additional lesion characterization. Axial oblique T2 (a) and T1-weighted images (b), sagittal T2-weighted images (c), contrast-enhanced T1-weighted images with fat saturation (FS) (d), gross specimen photography (e). A multilocular cystic mass of the right ovary (a) with a heterogeneous content in the most anterior loculation (*arrow*). The corresponding T1-weighted image (b) shows a hypointense content without any hemorrhagic portion excluding



**Fig. 9.2a,b.** Nonovarian cystic tumor. Transaxial (a) and coronal T2-weighted images (b) in a 14-year-old girl in whom sonography, to rule out an abscess after appendectomy, found a multicystic ovarian lesion. A large bilateral multiseptate lesion extending above the umbilical level is demonstrated in both planes. Identification of normal ovaries (*arrows*) allows exclusion of an ovarian origin of the lesion. Histopathology of the surgical specimen diagnosed a chyloma

the diagnosis of endometrioma. Sagittal T2-weighted image through the heterogeneous part of the cyst shows a hypointense solid portion (*arrow*) with converging thin septa of the cyst, possibly suggesting normal ovarian parenchyma (c). Contrast enhancement of the ovarian parenchyma and a slightly irregular interface between the cystic content and the wall of the cyst (*arrowheads*) is demonstrated in d. MRI diagnosed prospectively a benign multilocular tumor of the ovary without arguments for endometriosis. Gross specimen photography (e) of the right ovary shows a multilocular cyst with tiny papillary projections within the wall of the posterior loculation (*arrowheads*) and a white fibrous portion. Microscopic analysis diagnosed a benign serous cystadenofibroma of the ovary



**Fig. 9.3.** Beak sign. Transaxial T2-weighted images shows a mass in the left cul-de-sac (*asterisk*). Its ovarian origin can be clearly identified due to multiple follicles (*arrow*). The interface to the ovarian tissue is characterized by a sharp angulation, which is typical for the beak sign. A small amount of free fluid in the cul-de-sac as seen in this patient is a physiological finding in premenopausal age and peaks in the secretory phase



**Fig. 9.4.** Medial displacement of the iliac vessels. Transaxial CT in a patient with sonographically suspected bilateral ovarian cancer. Bilateral cystic lesions (*asterisks*) with mural thickening are simulating ovarian lesions. The displacement pattern of the iliac vessels, however, is typical for an origin from the pelvic sidewalls. The lesions present bilateral bursitis iliopectinea in a patient with rheumatoid arthritis

icking ovarian tumors, such as subserosal uterine leiomyoma. Furthermore, in the majority of leiomyoma cases, a vascular bridging sign at the interface between uterus and leiomyoma can be observed, which is not the case in ovarian lesions (Fig. 9.5) [13]. Because of their close anatomic relationship, masses arising from the fallopian tubes cannot be distinguished from ovarian lesions by identifying the ovarian vessels or the ovarian suspensory ligament [8]. However, incomplete septa emerging from the wall of a cystic adnexal mass indicate the fallopian origin of the mass (Fig. 9.6) [14].

## 9.4

### Characterizing Ovarian Lesions

#### 9.4.1

#### Differentiation Between Benign and Malignant Ovarian Lesions

Discrimination between benign and malignant ovarian tumors in patients who present with an adnexal mass is important for several reasons. It may directly affect the surgical decisions, including the adequate therapeutic

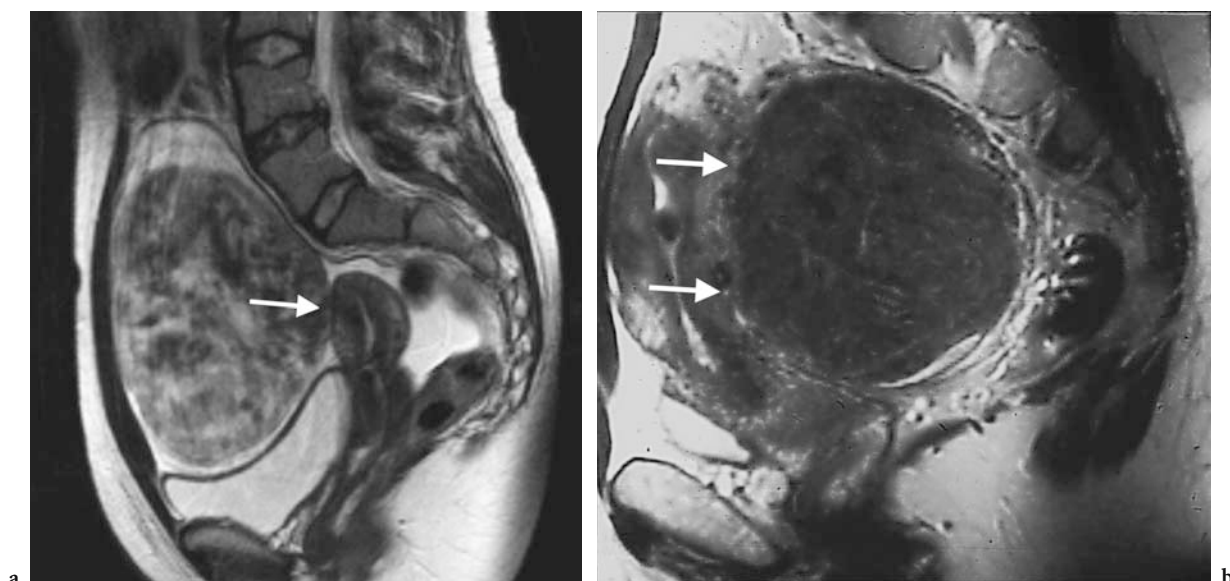


**Fig. 9.5a,b.** Ovarian vs extraovarian mass. Sagittal T2-weighted images demonstrate solid lesions adjacent to the uterus in two women of reproductive age. In ovarian fibroid (a), the uterus can be separated from the ovarian mass (*arrowhead*). Ascites is found in the cul-de-sac and surrounding the ovarian fibroid (a). A subserosal uterine fibroid (b) can be differentiated from an ovarian mass by demonstration of multiple bridging vessels. The latter (*arrows*) are found at the interface between the lesion and the myometrium

approach, surgical technique, and need of subspecialty cooperation. Furthermore, in times where endoscopic surgery has become very popular, thorough pretreatment evaluation should diminish the possibility of encountering an unexpected ovarian cancer [15].

The most commonly used criteria for differentiation between benign and malignant adnexal lesions do not differ between US, CT, and MRI. They include size, internal architecture of the mass, and assessment of additional signs suggestive of an invasive nature of the lesion, such as presence of lymphadenopathy and peritoneal implants, or ascites. Especially in sonography, more complex tests with multiparameter scoring systems, the combination of ultrasonographic characterization and Doppler findings and/or tumor markers have been suggested to improve performance [16, 17]. A multivariate analysis reported optimal lesion characterization when a combination of morphologic sonographic and color Doppler information is used (Fig. 9.7) [18]. Tumor size, wall thickness, and internal architecture, including the presence of septations, calcifications, papillary projections, and cystic and solid internal structures, have been established as diagnostic criteria for tumor characterization in all imaging modalities. At ultrasound, the presence of solid internal structures usually implies the use of



**Fig. 9.6.** Incomplete septations. Parasagittal T2-weighted images of a left adnexal mass. Incomplete interdigitating septa (*arrows*) are typical findings of a hydrosalpinx arising from the uterus. Widening of the fallopian tube to a diameter of 4 cm at the fimbriated end is seen

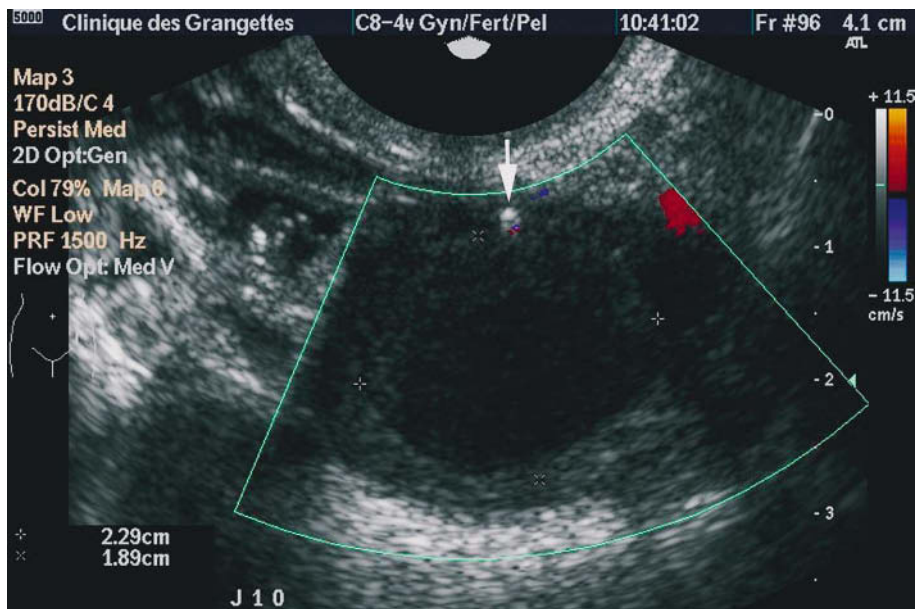


**Fig. 9.7.** Endometrioma with absent flow. A 34-year-old patient with chronic perimenstrual left pelvic pain. Sagittal transvaginal color Doppler sonographic image of the left ovary at day 10 of the menstrual cycle demonstrates a heterogeneous mass (between calipers) with two layers of internal low level echos, a wall calcification (*arrow*) and absent intracystic color Doppler flow. Pathology of the ovarian cyst diagnosed endometrioma

color Doppler ultrasound to identify the presence of intratumoral vessels indicative of solid tissue [19]. False-positive findings at ultrasound are possible using this specific diagnostic criteria because of the presence of vessels in solid structures in a wall thickening of a dermoid cyst, also called dermoid plug, which may contain tissue components of all three embryonic layers such as bone, lung, and skin tissue components [20]. Recognition of associated fat within the adnexal mass eases diagnosis of mature cystic teratoma. A second benign ovarian mass with solid tissue corresponds to ovarian fibromas and fibrothecomas characterized by mainly homogeneous solid tissue with a few small vessels and no or few associated cystic components (Fig. 9.8) [21].

At ultrasound, teratomas typically present as echogenic masses with acoustic shadowing due to hairballs or calcifications such as teeth or bone in the Rokitansky protuberance (Fig. 9.9) [22]. Layered lines and dots, the fat–fluid level, and isolated bright echogenic foci with acoustic shadowing are characteristic sonographic findings of dermoid cysts [23]. The majority of dermoid cysts can be reliably diagnosed by CT and MRI by the presence of intralesional fat. Endometriomas at ultrasound demonstrate diffuse low-level internal echos with hyperechoic foci

in the wall of a multilocular cyst [24]. The positive predictive value of sonography to predict endometriosis was evaluated at 75% when criteria such as diffuse low-level internal echos and absent neoplastic features were used. The use of color Doppler images helps to show absent flow within the sometimes heterogeneous cystic content. The presence of hyperechoic foci alone at the surface of the ovary is not a sign for endometriosis [25].

When CT and MRI are used, characteristics of malignancy can be best assessed in combination with contrast-enhanced studies [7, 26].

For all other ovarian lesions, features suggesting that a lesion is benign include lesion size less than 4 cm, entirely cystic architecture, wall thickness less than 3 mm, lack of internal structures, lack of ascites, and lack of peritoneal disease or lymphadenopathy. Using these criteria, MRI has been shown to have a 91%–95% accuracy for differentiating benign from malignant adnexal tumors [7, 27, 28]. Particularly the presence of papillary projections within an ovarian lesion should raise the suspicion of malignancy [19]. The presence of necrosis within a solid portion of an ovarian mass was most predictive of malignancy in a multivariate logistic regression analysis in a population of patients with complex sonographic adnexal

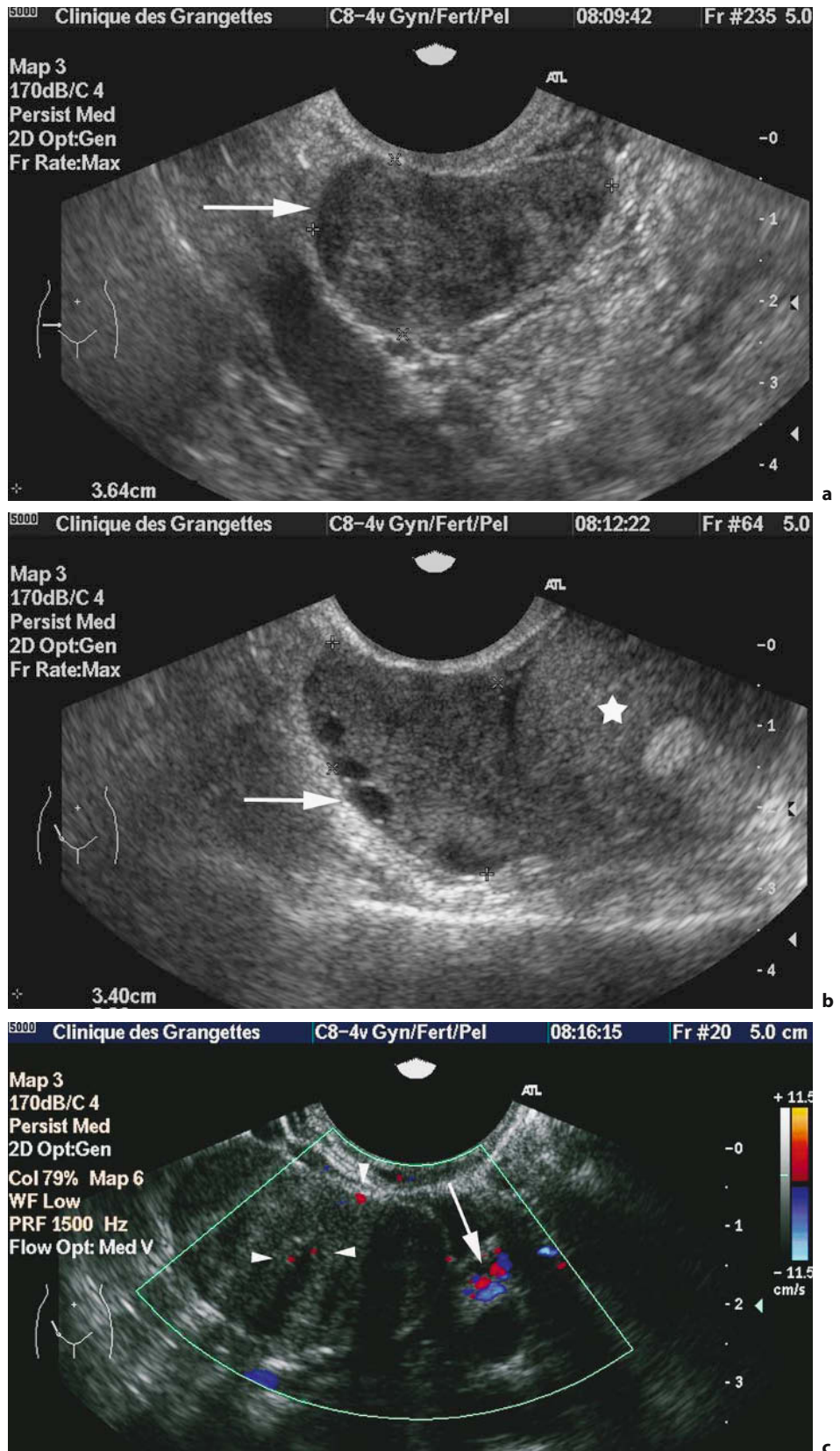


**Fig. 9.8a–c.** Fibroid on US: a 40-year-old patient with a right adnexal mass at physical routine examination by the gynecologist. Transvaginal US in axial, axial oblique (a), and sagittal oblique (b) plane. A 36-mm circumscribed heterogeneous oval mass (arrow) is demonstrated close to the right external iliac vessels (a) A more oblique orientation identifies a separate normal-appearing right ovary (arrow) close to the uterus (star, b). Color Doppler image (c) shows both the right ovary with parenchymal ovarian vessels (arrow) and the adjacent solid mass with tiny vessels (arrowheads). No vascular communication is seen between the ovary and the right-sided solid mass. Subsequent surgery and pathology confirmed leiomatoma of the right large ligament



**Fig. 9.9a-c.** Dermoid on transvaginal sonography. Axial transabdominal US (a), transvaginal sagittal US (b), color Doppler US (c) in a 40-year-old woman with incidental left adnexal mass during ultrasound for intrauterine device change. Axial transabdominal ultrasound (a) of the pelvis demonstrates a left adnexal mass posterior to the uterus containing an intrauterine device. The left adnexal mass is isoechoic to the myometrium and contains a hyperechoic peripheral portion with posterior attenuation, suggesting calcification. The transvaginal sagittal image of the mass (b) shows an ovally shaped, well-circumscribed mass with hyperechoic content and wall-simulating bowel. The color Doppler transvaginal image (c) demonstrates utero-ovarian vessels providing blood flow to the compressed triangular ovarian parenchyma indicated by calipers at one pole of the mass. The cystic content of the heterogeneous hyperechoic ovarian mass is confirmed by absent intracystic color flow. Subsequent laparoscopy confirmed mature cystic teratoma

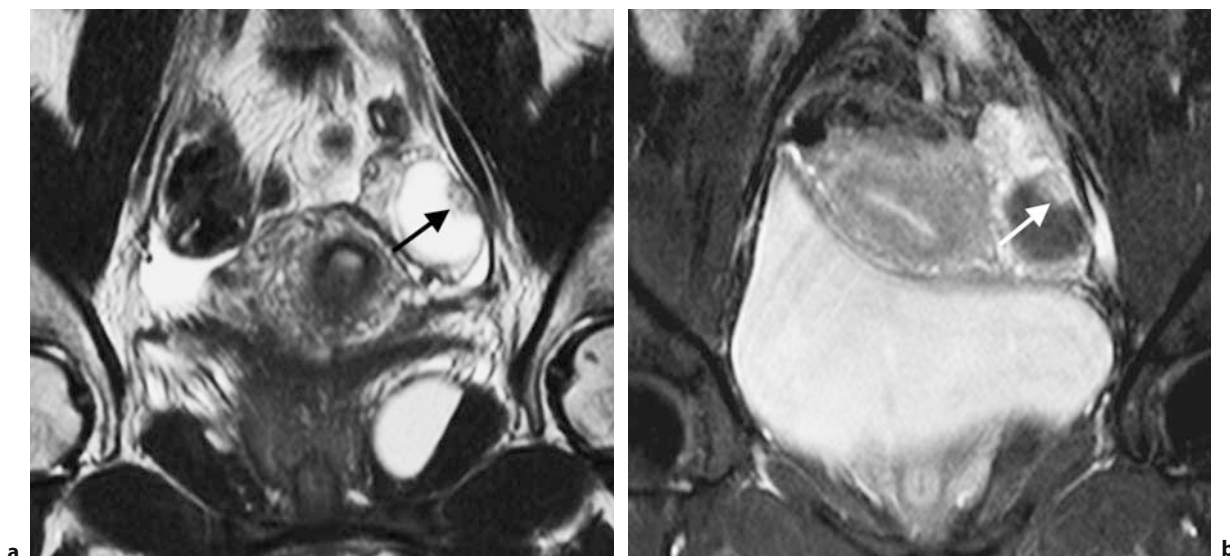


**Fig. 9.10a,b.** Vegetation within a cyst. Coronal T2-weighted images (a) and contrast-enhanced T1-weighted images with FS (b). In a 3.5-cm ovarian cyst, a mural nodule of 10 mm with low signal intensity on T2-weighted images (a) and contrast enhancement (b) is demonstrated. This finding should warrant the suspicion of malignancy, especially a borderline tumor as in this patient. Papillary projections in cystadenomas tend to be smaller

masses undergoing MRI for lesion characterization. “Necrosis in a solid lesion” (odds ratio, 107) was followed by “vegetations in a cystic lesion” (odds ratio, 40) identified after intravenous injection of gadolinium-based contrast material (Fig. 9.10). Interobserver (K, 0.79–0.85) and intraobserver (K, 0.84–0.86) agreement were excellent [7].

Calcifications can be easily detected in CT, whereas they are difficult to appreciate on MRI. Calcifications within the wall or the dermoid plug are a typical finding in dermoid cysts. Dense calcifications are often found in benign stromal tumors in middle-aged women. Psammoma bodies found at histologic examination in up to 30% of malignant serous tumors present a subtle finding on CT with tiny amorphous calcifications [29].

The malignancy rate in completely cystic masses in postmenopausal women is extremely low (less than 1%–2%) (Fig. 9.11) [30]. The probability of malignancy is related to lesion size. GOLDSTEIN et al. did not find cancers in cystic lesions less than 5 cm in size in postmenopausal women, and RULIN and PRESTON found in 150 ovarian masses in the same age group to be cancers in only 3%, when the size was less than 5 cm, and they were cancers in 11% of lesions with a diameter between 5 and 10 cm; however, 63% of lesions larger than 10 cm were malignant [31, 32].

Ascites alone is nonspecific with small amounts of pelvic fluid typically detected in the cul-de-sac (Fig. 9.3). Only larger amounts of pelvic fluid may be

an important ancillary finding to support the diagnosis of peritoneal spread in malignancy. Peritoneal enhancement is a pathologic finding, but is not specific and is associated with benign and malignant diseases [33]. Absence of ascites in the cul-de-sac in cases of ascites throughout the pelvis or abdomen has been described as a sign of malignancy [34].

The probability of malignancy is also related to the patient’s age. In girls less than 9 years of age, 80% of ovarian masses are malignant, with the majority consisting of germ cell tumors. In women of reproductive age, the overall chance that an ovarian tumor will be malignant is 1 in 15 compared to 1 in 3 by 45 years of age [35].

#### 9.4.2 Functioning Ovarian Tumors

Clinical and imaging findings may lead to the diagnosis of a functioning ovarian tumor.

The imaging findings comprise an ovarian mass, but also indirect findings as abnormalities of the uterus with uterine enlargement, a thickened endometrium in pre- and postmenopausal women, abnormal bleeding, features of virilization or endocrinologic symptoms [36].

Sex cord stromal tumors account for the majority of functioning ovarian tumors. These benign masses

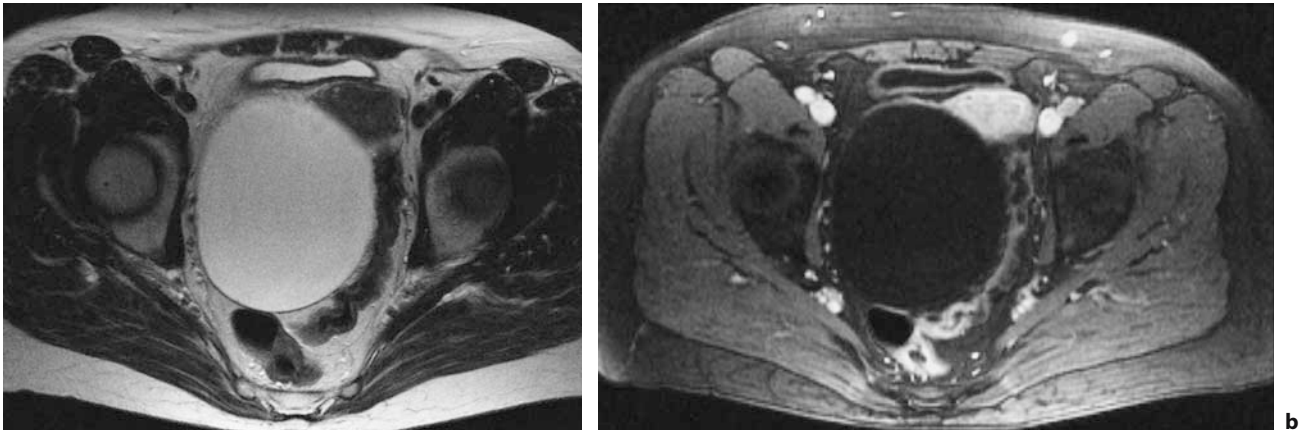


**Fig. 9.11a,b.** Large cystic adnexal lesion in a 55-year-old woman. Transaxial T2-weighted images (a) and T1-weighted images with fat saturation (b) show a unilocular right adnexal cyst. It displaces the uterus and the adjacent sigmoid colon. Imaging criteria include no evidence of malignancy. Due to postmenopausal age and the increase in size, surgery was performed. The histopathological diagnosis was serous cystadenoma

as well as neoplasms of low malignant potential account for the majority of estrogen-producing tumors. Granulosa cell tumors and the benign thecomas are the most common estrogen-producing tumors (Fig. 9.12). Some mucinous cystadenomas, and rarely ovarian cancer and metastases may also produce estrogens [37]. In the majority of women of reproductive age, virilization is associated with the benign disorder polycystic ovaries disease (PCOS). Virilizing ovarian tumors are rare, typically solid ovarian tumors [38]. Sertoli Leydig cell tumors are typically found in young women and account for two-thirds of these tumors causing hirsutism or virilization. In middle-aged women, steroid cell tumors can cause virilization and/or Cushing's syndrome. Further-

more, rarely granulosa cell tumors, Brenner tumors, and fibrothecomas may also have virilizing effects.

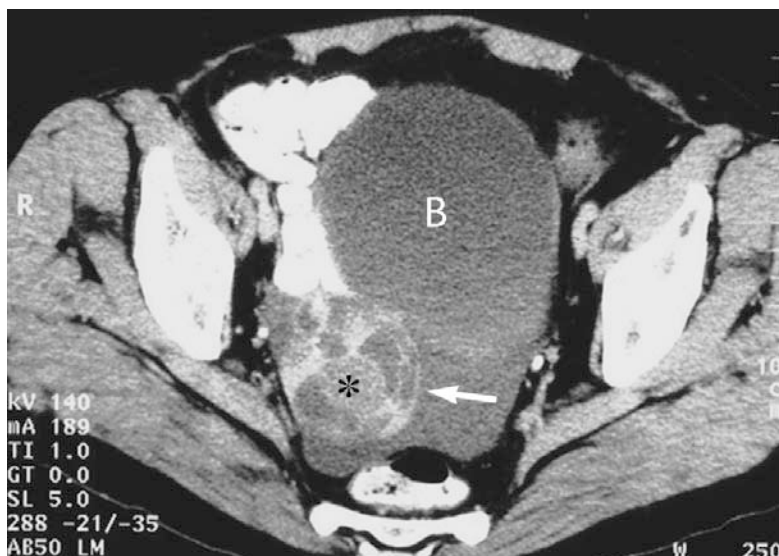
In addition to the sex-cord stromal tumors, a variety of other benign and primary and metastatic malignant ovarian tumors may have a functioning stroma with estrogenic or androgenic production. However, these elevations will remain commonly subclinical. These tumors include mucinous tumors, rarely endometrioid carcinoma, malignant germ cell tumors, and mucinous metastatic carcinomas [37].

Thyroid hormones are typically produced in struma ovarii and struma carcinoids of the ovary in subclinical levels. Hyperthyreosis seems to be present in only 25%, and thyrotoxicosis occurs in only 5% of patients with struma ovarii (Fig. 9.13) [37]. Primary



**Fig. 9.12.** Granulosa cell tumor. A 52-year-old female with a history of hysterectomy and unilateral oophorectomy for granulosa cell tumors several years before. A solid and cystic pelvic tumor with irregular margins displacing bowel loops is seen at the acetabular level. From imaging, it cannot be differentiated from an ovarian cancer

**Fig. 9.13.** Struma ovarii. Transaxial CT in a young woman who presented with a complex adnexal mass at sonography and no evidence of hyperthyreosis. A left adnexal (*arrow*) surrounded by ascites is demonstrated in the cul-de-sac. It is well defined, shows a thin wall, and demonstrates a solid and cystic architecture. Within the lesion a locule (*asterisk*) of high density presents hemorrhage. B, bladder. Courtesy of Dr. T.M. Cunha, Lisbon



carcinoids of the ovary are rarely associated with carcinoid syndrome. Metastatic carcinoids involving the ovary, however, are associated with carcinoid syndrome in 50% of cases. Benign and malignant mucinous ovarian tumors may produce gastrin within the cyst wall and present clinically with Zollinger-Ellison syndrome [39].

#### 9.4.2.1

##### Value of Imaging

The value of imaging in patients with clinically suspected functioning ovarian tumors is to rule out an adnexal mass. In case of virilization, it may also confirm the diagnosis of polycystic ovaries, and rule out an adrenal mass by thorough assessment of the adrenal glands.

#### 9.4.3

##### Ovarian Tumors in Children, Adolescents, and Young Women

Imaging findings, age, and clinical presentation of ovarian masses in infants and young women are the basis of treatment strategy. In this age group – unless there is histologically proven malignancy – conservative ovarian surgery and preservation of fertility is a special concern.

The type of ovarian tumor depends on the morphology and patient's age. The majority of ovarian masses in children older than 9 years and young

women are benign and include follicular cysts and dermoid cysts, with fewer than 5% of ovarian malignancies occurring in this age group. However, lesions with complex architecture should be carefully assessed, as 35% of all malignant ovarian neoplasms occur during childhood and adolescence. This is especially true for children younger than 9 years, where approximately 80% of ovarian neoplasms are malignant [40]. A solid ovarian mass in childhood should also be considered malignant until proven otherwise by histology [41]. Differential diagnosis includes dysgerminoma, neuroblastoma (Fig. 9.14) rhabdomyosarcoma, lymphoma, and nongenital tumors in the pelvis. Some ovarian neoplasms occurring in this age group excrete protein tumor markers, which may aid in diagnosis and follow-up. They include alpha-fetoprotein, which is produced by endodermal sinus tumors, mixed germ cell tumors, and immature teratomas, lactate dehydrogenase, which is secreted by dysgerminomas, and human chorionic gonadotropin, which is elevated in pregnancy and pregnancy-related tumors and in embryonal ovarian carcinomas [41]. Torsion is a special problem in children and young adults presenting with an ovarian mass. Usually ovarian masses associated with torsion are benign cystic lesions (Fig. 9.15); particularly lesions presenting with a size greater than 5 cm seem to be under a special risk for torsion [42]. Acute pelvic pain is the mainstay in the differential diagnosis of a torsed ovary; however, imaging findings may be misleading and simulate a malignant ovarian tumor.

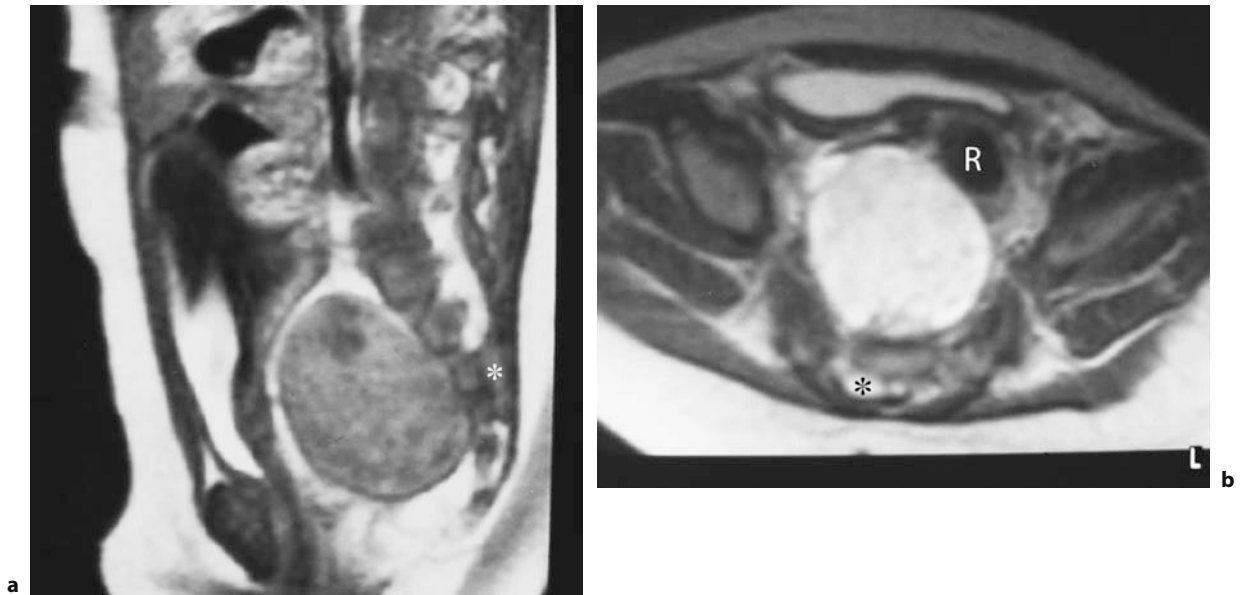


**Fig. 9.14a,b.** Pelvic neuroblastoma. Sagittal contrast-enhanced T1-weighted images (a) and transaxial T2-weighted images (b) of a 5-month-old girl with a sonographically detected right pelvic mass. A well-delineated solid tumor with moderate inhomogeneous contrast enhancement (a) and bright signal on T2-weighted images (b) is seen in the posterior aspect of the pelvis. It compresses the bladder and displaces the rectum (R) anteriorly and to the left side. Furthermore, a small lesion (asterisk) with the same signal intensity as the tumor is seen in the sacral canal at the level of S3. At surgery, a neuroblastoma was resected, which was composed of a small intraspinal and a large pelvic tumor component



**Fig. 9.15.** Torsion of a paraovarian cyst. In a 14-year-old girl with severe acute pelvic pain a cystic lesion was found on sonography. CT shows normal ovaries in the ovarian fossa and a 7-cm cystic lesion (asterisk) in the cul-de-sac. The latter shows mild wall thickening at its left contour. Exploratory laparotomy found torsion of a right paraovarian cyst with involvement of the right fallopian tube. The ovaries were unremarkable

Ovarian cysts are uncommon before puberty. Most of these are physiologic follicular cysts that will resolve spontaneously. Some ovarian cysts may be hormonally active and result in precocious pseudopuberty, e.g., in McCune-Albright syndrome [43]. Development of cysts is extremely common between puberty and 18 years of age. Most of these cysts are functional ovarian cysts and may attain a size of up

to 8–10 cm. In this age group, paraovarian or mesothelial cysts, hydrosalpinx, tubular pregnancy, and obstructive genital lesions may also simulate cystic ovarian lesions. Germ cell tumors account for half to two-thirds of the tumors in girls up to 18 years; they present 70% of ovarian tumors in the age between 10 and 30 years [44]. The vast majority are unilateral and present dermoid cysts. Only 3% of ovarian germ

cell tumors are malignant. Dysgerminomas account for approximately 50% of the malignant germ cell malignancies in adolescents and young adults and are followed by endodermal sinus tumors (20%) and immature teratomas (19%). As in many ovarian malignancies, rapid growth is a typical finding; however, bilateral manifestation is more common in dysgerminomas than in other malignant germ cell tumors.

Endodermal sinus tumors are found in women at a median age of 18 years, often diffuse peritoneal dissemination is already present at the time of diagnosis [45].

Juvenile granulosa cell tumors are stromal cell tumors of low malignant potential, which occur before the age of 30. Rarely, they occur before puberty and may become clinically apparent as precocious puberty. Immature teratomas are commonly associated with a mature teratoma; they comprise 1% of all teratomas and occur most commonly in the first two decades of life. Tumor markers are usually negative [46].

#### 9.4.3.1

##### Value of Imaging

Sonography is the modality of choice to determine the architecture of a suspected ovarian mass in children and young adolescents. The sonomorphologic pattern in combination with age, clinical manifestation and presence of tumor markers are pivotal to establish the diagnosis. Cystic lesions are usually followed and regress in the majority of cases. In case of growth, or presence of a complex cystic or solid ovarian lesion, further characterization by CT or MRI is usually performed (Fig. 9.2). The information obtained includes complementary evaluation of the site of origin, the nature of the mass (presence of fat or calcifications), and metastases. Because of radiation issues, MRI is the preferred imaging modality in this age group.

The imaging characteristics in CT and MRI of the different tumors are discussed in detail in this and Chap. 10.

#### 9.4.4

##### Adnexal Masses in Pregnancy

With the widespread use of abdominal ultrasound during pregnancy, adnexal masses are concurrently diagnosed with increasing frequency. Adnexal masses

have been reported to occur in 0.15%–1% of pregnancies. Most patients are asymptomatic at the age of presentation, and most adnexal masses disappear during the first 16 weeks of pregnancy [47]. The incidence of ovarian cancer associated with a persistent adnexal mass varies from 3% to 5.9% (Fig. 9.16). In a retrospective analysis of 60 adnexal masses during pregnancy, 50% included mature cystic teratomas, 20% cystadenomas, 13% functional ovarian cysts, and 13% malignant tumors. Among the latter, six out of eight were tumors of low malignant potential, and all malignant lesions were FIGO stage Ia tumors [48]. The therapeutic regimen of an adnexal mass during pregnancy depends on the size, sonomorphologic criteria, and gestational age. Lesion size seems to play an important role in the management of adnexal masses during pregnancy. Many authors recommend conservative treatment in adnexal masses 6 cm or smaller [48]. The vast majority of these are cysts, which will resolve spontaneously. Furthermore,

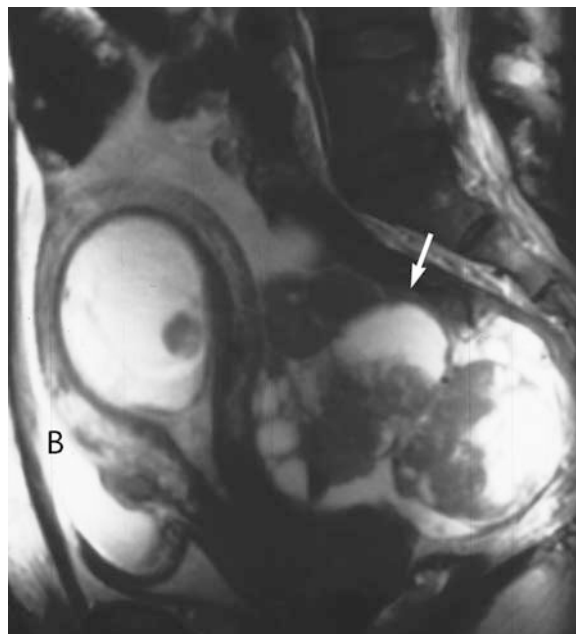


**Fig. 9.16.** Ovarian cancer in pregnancy. In a 38-year-old woman who underwent routine sonography during pregnancy, a suspicious adnexal lesion was found. Sagittal T2-weighted images shows dilatation of the uterine cavity and the fetus. A large solid and cystic adnexal mass is demonstrated located posterior and above the uterine cervix, compressing the rectum. Ascites is demonstrated in the upper pelvis, but not in the cul-de-sac. Surgical staging showed stage III ovarian cancer. *B*, compressed bladder

the risk of torsion of an ovarian mass of this size seems low.

SHERARD et al. reported an average size of 11.5 cm in malignant lesions, in contrast to benign lesions, which showed an average size of 7.6 cm [48]. Furthermore, papillary projections were a typical finding of borderline tumors.

Pain or an acute abdomen should alert to complications due to hemorrhage, rupture, and torsion of the adnexal mass (Fig. 9.17) or caused by nongynecological pelvic diseases.

#### 9.4.4.1

##### Value of Imaging

Adnexal masses during pregnancy are often incidental findings during fetal sonography. Sonography is the modality of choice to further characterize these masses, assess their size, and plan follow-up. The aim of thorough assessment of an adnexal mass during pregnancy is to manage typical benign masses conservatively and/or to postpone surgery in the second or third trimester in order to reduce adverse fetal outcome. MRI has been used to characterize masses in pregnancy [49]. It is particularly useful to further characterize sonographically solid lesions, especially to exclude a leiomyoma and confirm the diagnosis of a dermoid. In patients with acute abdomen, MRI is also used as a complement to sonography to detect nongynecological causes, e.g., appendicitis or enteritis [50].

## 9.5

### Benign Adnexal Lesions

#### 9.5.1

##### Non-neoplastic Lesions of the Ovaries and Adnexa

##### 9.5.1.1

##### Physiologic Ovarian Cysts

The ovaries change their appearance periodically during their ovarian cycle. The ovarian cycle consists of development of the ovarian follicle, rupture, discharge of the ovum, formation and regression of corpus luteum.

Ovarian cysts under 3 cm are regarded as physiologic cysts. They include follicles of various stages of development, corpus luteum cysts, and surface inclusion cysts.

Physiologic ovarian cysts constitute the vast majority of cystic adnexal lesions. They may be classified as functional, which means they are associated with hormone production, or nonfunctional.

They occur typically in women in the reproductive age; however, less commonly they may be also found in the postmenopausal age. In a series of 74 normal ovaries, the average size of the largest cyst was 1 cm (range, 0.2–4.7 cm) [51]. Functional cysts usually do not exceed 5 cm in size, but may occasionally grow as large as 8–10 cm (Fig. 9.18). In most cases, they are

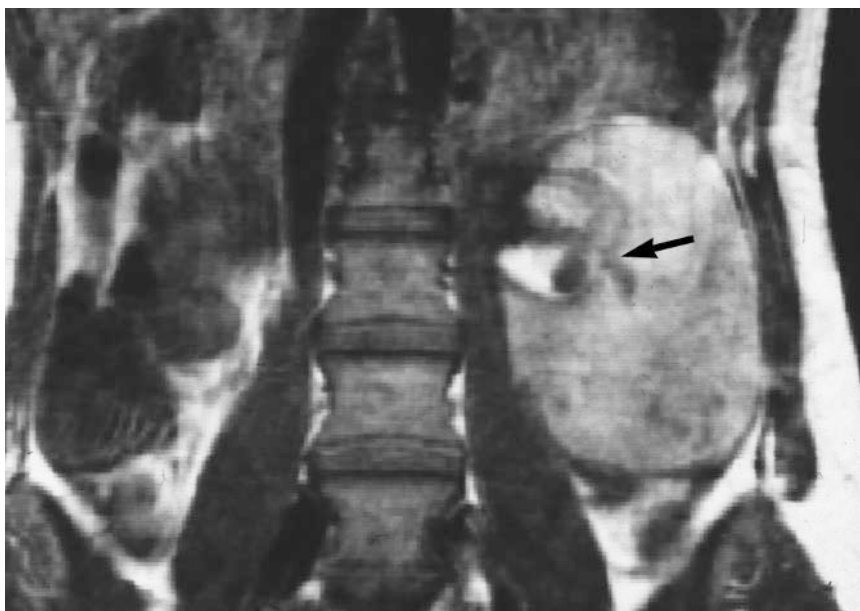


**Fig. 9.17.** Torsion of a dermoid. MRI was performed in a woman presenting with acute pelvic pain in the 16th week and an indeterminate mass at sonography. Coronal T1-weighted images shows a well-delineated mass 15 cm in diameter with high SI due to hemorrhage in the left mid abdomen. At its mediocranial aspect, an apple-like structure also containing very bright signal presents the Rokitansky nodule (*arrow*). Dilatation of the fallopian tube, which is a common associated finding in adnexal torsion, is demonstrated at the inferior margin of the lesion. At surgery, hemorrhagic infarction of the dermoid and left adnexa was found

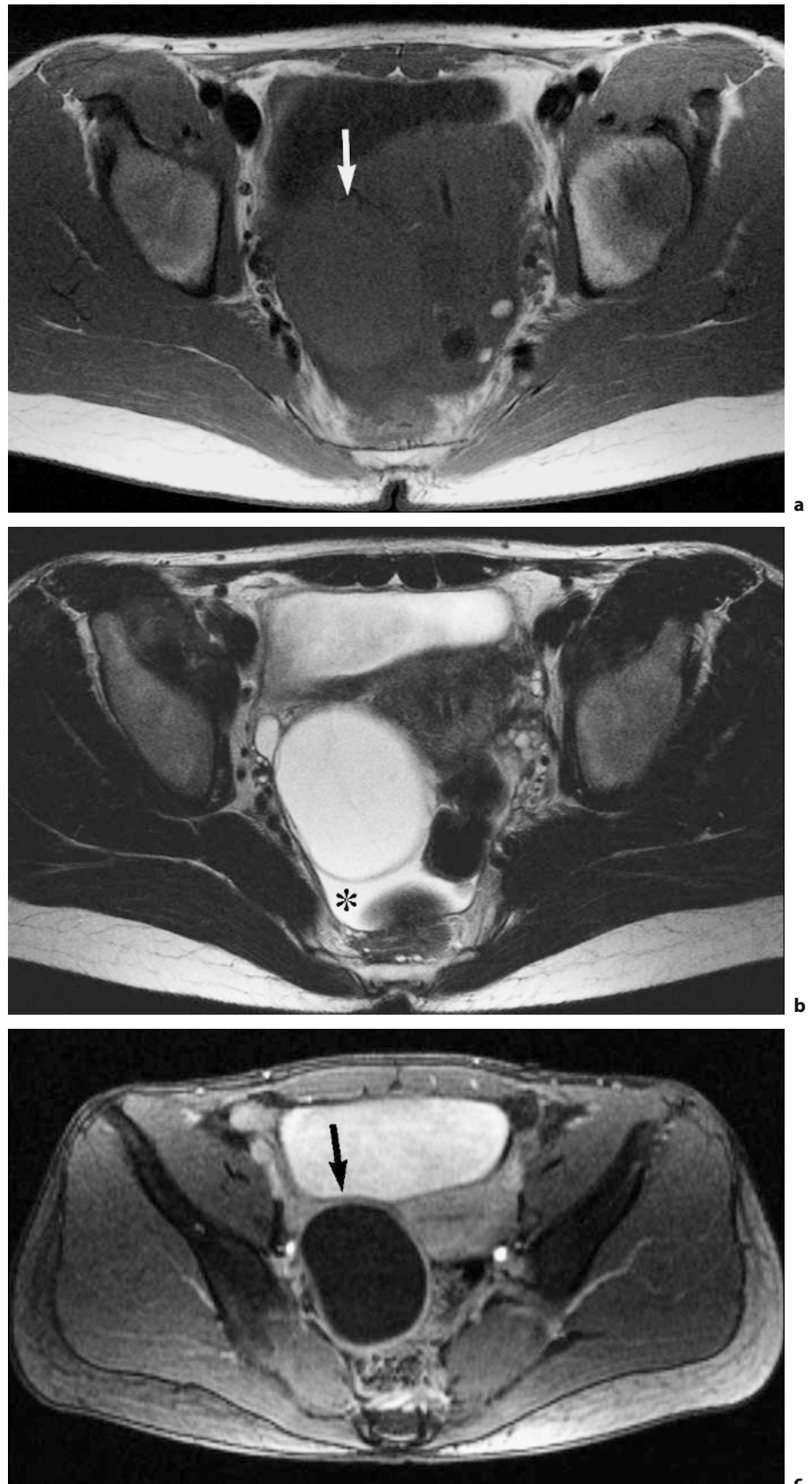


**Fig. 9.18a–c.** Functional cyst in a 29-year-old woman. Transaxial T1 (a), T2-weighted images (b) and contrast-enhanced T1-weighted images with FS (c). An 8-cm cystic ovarian lesion (*arrow*) with intermediate signal intensity on T1-weighted images similar to myometrium (a), and very high SI on T2-weighted images (b) displays a thin wall on the T2-weighted images (b) and after contrast administration (c). From imaging, a functional cyst, most likely a corpus luteum cyst, could not be differentiated from a cystadenoma. The sonographic follow-up showed a considerable decrease in size within 3 months. Small amount of ascites in the cul-de-sac

self-limiting and will regress spontaneously. In contrast to follicular cysts, corpus luteum cysts often require a period of up to 3 months to regress.

#### 9.5.1.1.1

##### **Follicular and Corpus Luteum Cysts**

The majority of ovarian cysts are follicular cysts resulting from failure of rupture or of regression of the Graafian follicle. Under nonpregnant conditions, corpus luteum cysts derive from failure of regression or hemorrhage into the corpus luteum.

Functional cysts are asymptomatic in the majority of cases. Progesterone production may persist in corpus luteum cysts, resulting in delayed menstruation or bleeding anomalies. Large physiologic cysts may cause abdominal pressure or low back pain. Acute abdomen is caused by complications such as rupture, hemorrhage, or torsion.

#### 9.5.1.1.2

##### **Imaging Findings in Physiologic Ovarian Cysts**

Transvaginal sonography is currently the gold standard for the diagnosis of ovarian cysts. Findings include anechoic thin walled cysts for simple follicular cysts and a fishnet like heterogeneous hypoechoic content for hemorrhagic follicular or luteal cysts also described with a fine trabecular jelly-like content (Fig. 9.19) [52]. Most of these cysts will disappear or decrease in size at short-term follow-up. In all, 65% of the cysts persisting after menstruation had resolved

at the first control examination 3 months later, independently of the use of oral contraceptives [53].

Simple ovarian cysts are a common incidental finding in CT and MRI. They are unilocular and display an imperceptible or thin (<3 mm) wall. On CT they appear as round or oval water-density lesions (<20 HU). Most cysts display intermediate to low signal intensity (SI) on T1-weighted images, and very high signal intensity on T2-weighted images, due to presence of simple fluid. The thin wall is best depicted on T2-weighted images as hypointense and on contrast enhanced images as hyperintense to ovarian stroma [51]. Hemorrhagic ovarian cysts and corpus luteum cysts tend to display a high SI on T1 and intermediate to high SI on T2-weighted images [51]. Corpus luteum cysts tend to have thicker walls than follicle cysts, with distinct enhancement due to their thick luteinized cell lining. Layering by debris and internal fibrin clots in corpus luteum cysts can be differentiated from papillary projections in epithelial tumors by their lack of enhancement.

#### **Differential Diagnosis**

Functional cysts smaller than 2.5-3 cm cannot be differentiated from normal mature follicles. Unilocular cystadenomas may mimic functional cysts. Regression in a follow-up over two to three cycles, however, will allow the diagnosis of a nonneoplastic functional cyst. Unilocular cystic lesions even in postmenopausal women have an extremely low incidence of malignancy (Fig. 9.11) [32].

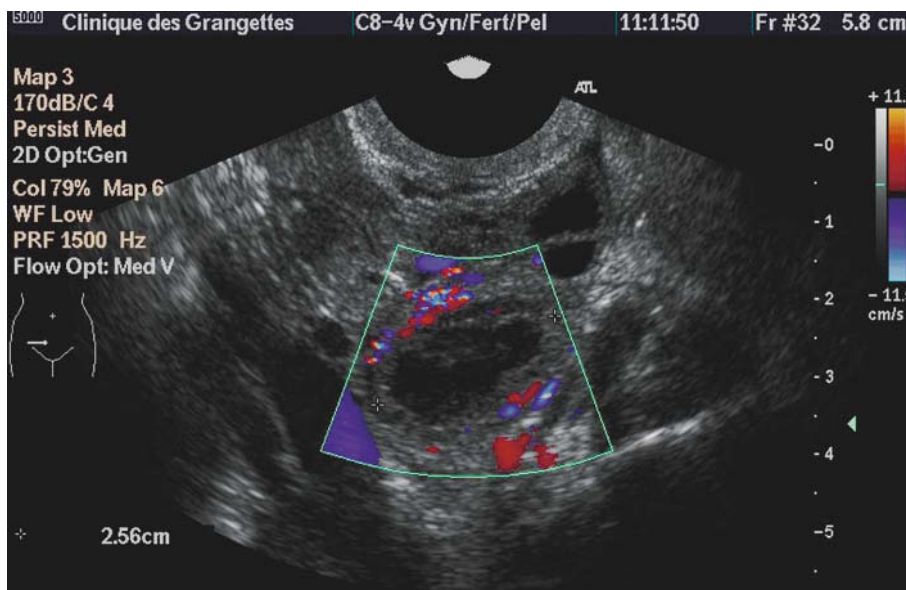


**Fig. 9.19.** Corpus luteum cyst in sonography. A 35-year-old woman with recent right pelvic pain. Axial transvaginal sonographic image of the right ovary shows a 25-mm ovarian cyst with hypoechoic heterogeneous content, an irregular wall, absent intracystic color Doppler flow, and increased peripheral blood flow within the ovarian parenchyma, suggesting a corpus luteum cyst. Findings were confirmed at a follow-up sonography 3 months later, demonstrating a normal right ovary

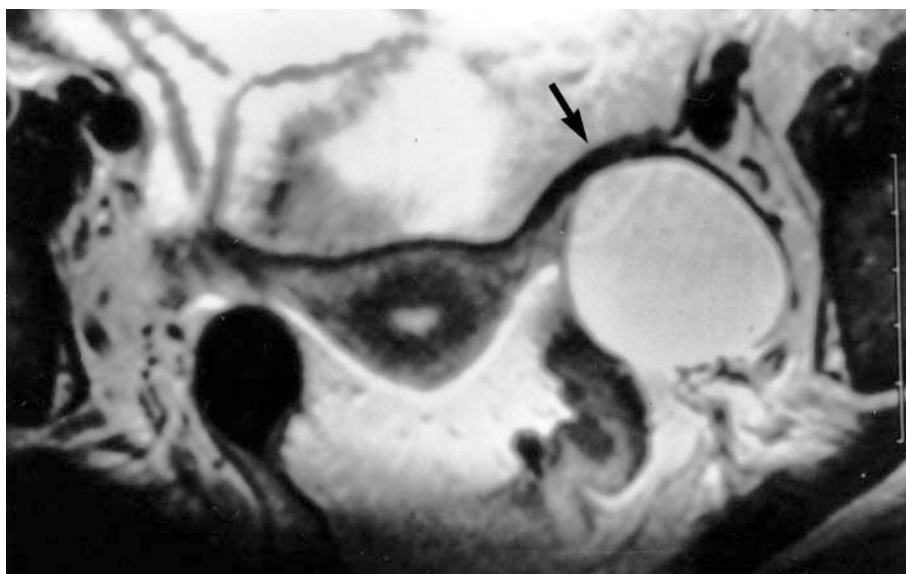


**Fig. 9.20.** Paraovarian cyst. Transaxial T2-weighted images shows a thin-walled cyst (*arrow*) displacing the left adnexa. Not histologically verified

Both corpus luteum cysts and endometrioma may show intracystic hemorrhage; however, only in endometrioma will a prominent T2 shortening (“shading”) be observed [54]. Furthermore, in endometriosis often multiple hemorrhagic cysts may be found.

#### 9.5.1.2

##### Paraovarian Cysts

Paraovarian cysts (paratubal) cysts arise from Wolffian duct remnants in the mesovarium [2]. They are often an incidental finding. Although encountered throughout life, they are most commonly found in middle-aged women. Surgical data suggest that they account for 10%–20% of adnexal masses [55]. They are round or ovoid, unilocular thin-walled cysts with a wide range of sizes between 1 and 12 cm; several have been reported as large as 28 cm [56]. Complications do not differ from those of functional ovarian cysts. Secondary transformation with foci of benign and malignant papillary neoplasms is extremely rare [57].

#### 9.5.1.2.1

##### Imaging Findings

Paraovarian cysts tend to be large thin-walled unilocular cysts, located typically within the broad ligament (Fig. 9.20). Rarely they may contain internal septations. On CT and MRI, they display typical criteria of ovarian cysts, but are found separate from the ipsilateral ovary [55, 58].

#### 9.5.1.2.2

##### Differential Diagnosis

A paraovarian cyst can only be distinguished from an ovarian cyst if it is clearly separate from the ovary. While paraovarian cysts are usually larger cysts, cysts of Morgagni, which arise from the fimbriated end of the tube, usually do not exceed 1 cm in diameter. The differential diagnosis of paraovarian cysts includes ovarian cystadenoma, an eccentric ovarian cyst, retroperitoneal cysts, and lymphoceles. The latter can be differentiated based on the clinical history and the pattern of vascular displacement. Hydrosalpinx may have a similar location within the broad ligament; however, it displays a tubular form and interdigitating septa. In contrast to paraovarian cysts, peritoneal inclusion cysts are often not round, but their shape is defined by the surrounding structures. Complicated paraovarian cysts cannot be differentiated from abscesses, endometriomas, and even ovarian cancer.

#### 9.5.1.3

##### Peritoneal Inclusion Cysts

Peritoneal inclusion cysts (pseudocysts) are accumulations of fluid produced by the ovaries that become entrapped by peritoneal adhesions. These lesions are typically encountered in patients with previous surgery, endometriosis, or pelvic inflammatory disease (PID). They are of variable size and tend to adhere to adjacent structures. Pseudocysts have an irregular shape because the outer surface is not a true wall but

defined by surrounding structures. They may become clinically apparent due to mass effect, pain, or present without symptoms [56].

#### 9.5.1.3.1

##### **Imaging Findings**

Peritoneal inclusion cysts tend to take the shape of the space they are occupying, and may displace surrounding structures. The ovary or tubes lie typically inside or inside the cyst wall and may be mistaken as a solid nodule (Fig. 9.21). The internal architecture of peritoneal inclusion cysts depends on the contents. In most cases, they contain simple fluid with low SI on T1-weighted images and very high SI on T2-weighted images, and low density on CT. Hemorrhage and layering of hemosiderin can lead to high SI on T1 and low SI on T2 W, and higher densities on CT. In one study internal septa were found in 11/15 cases of peritoneal inclusion cysts [56].

#### 9.5.1.3.2

##### **Differential Diagnosis**

Septations within a peritoneal inclusion cyst, the murally located ovary mimicking a solid component within a cystic mass, and distortion of pelvic anatomy

may make the differentiation from a malignant ovarian tumor difficult. The coverage of adjacent organs and the history of a previous surgery or pelvic adhesions may be key arguments for the correct diagnosis [59].

#### 9.5.1.4

##### **Theca Lutein Cysts**

Theca lutein cysts are ovarian cysts that are lined by luteinized theca cells. They develop in patients with high levels of serum human chorionic gonadotropin. They are not as common as other ovarian cysts. They are associated with multiple gestations, trophoblastic disease, and pregnancies complicated by hydrops fetalis, or in ovarian hyperstimulation syndrome.

#### 9.5.1.4.1

##### **Imaging Findings**

Theca lutein cysts are typically large, bilateral multiseptate ovarian cysts composed of simple fluid. They may cause gross enlargement of the ovaries to 10–20 cm in diameter. T2-weighted images or contrast-enhanced MRI or CT will typically display no evidence of mural thickening (Fig. 9.22).

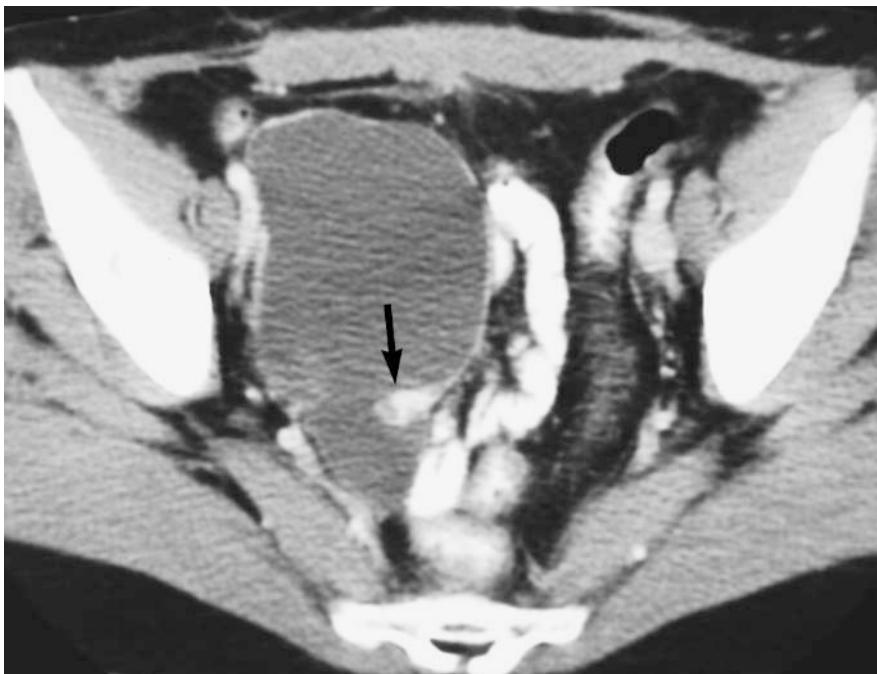


**Fig. 9.21.** Peritoneal inclusion cyst. In a 33-year-old woman with a history of several previous pelvic surgeries, a cystic lesion of the right adnexa was found at sonography. CT demonstrates a cystic lesion with thin enhancing walls and a solid ovoid structure (*arrow*) at its posterior wall. Surgery revealed an inclusion cyst, the solid structure presented the normal ovary

#### 9.5.1.4.2

##### **Differential Diagnosis**

Theca lutein cysts may resemble bilateral cystadenomas; however, the clinical background is different.

#### 9.5.1.5

##### **Polycystic Ovary Syndrome**

Polycystic ovary syndrome (PCOS) is a complex endocrinologic disorder characterized by inappropriate gonadotropin secretion that results in chronic anovulation [60]. It affects as many as 5%-10% of women of reproductive age, and is found in 50% in women with infertility problems [61].

Although most notable in Stein-Leventhal syndrome, which comprises the classical findings of amenorrhea, hirsutism, obesity, and sclerotic ovaries, a wide range of clinical presentations exist. Only one-quarter to one-half of the patients present the classical signs. Usually, infertility is the leading clinical problem of patients with PCOS. Recently, ultrasonographic studies reported a prevalence of polycystic ovaries in young women of at least 20%. However, there seems to be an overlap of polycystic ovaries and normal ovaries [62].

An increased risk of endometrial cancer in patients has been noted in patients with PCOS younger than 40 years of age due to chronic estrogen stimulation [63]. PCOS may also be associated in women with venous congestion who suffer from pelvic pain [64].

The morphologic hallmark is mild enlargement of both ovaries, which contain multiple small cysts surrounding the increased central ovarian stroma. The follicles may concurrently exist in different stages of growth, maturation, or atresia.

#### 9.5.1.5.1

##### **Imaging Findings**

As there seems to be an overlap of normal and polycystic ovaries in imaging, the diagnosis of polycystic ovary syndrome is based on hormonal changes as well as clinical and imaging findings [65].

The imaging modality of choice is transvaginal US [55]. MRI is used as a complement to US to confirm the diagnosis of PCOS or to exclude a virilizing ovarian tumor.

The imaging findings in PCOS include bilateral moderately enlarged (up to 5 cm) spherical ovaries with an abnormally high number of follicles (Fig. 9.23). These follicles are typically found in a peripheral distribution. At least ten follicles ranging between 2 and 8 mm in size encircle the abnormally hypointense central stroma (Fig. 9.24). A dominant follicle is typically not seen [66]. Rarely, a normal contralateral ovary may be identified. The ovaries are surrounded by a thickened sclerotic capsule and typically display abundant low signal central stroma on T1- and T2-weighted images (Fig. 9.24).

**Fig. 9.22.** Bilateral theca lutein cysts CT at the umbilical level in a 27-year-old patient with a hydatiform mole. Bilaterally enlarged ovaries are demonstrated displaying numerous thin-walled cysts of water-like density. No enhancing solid structures or papillary projections could be identified. Theca lutein cysts are found in up to 20% of patients with a hydatiform mole





Fig. 9.23. Polycystic ovaries in CT. Bilateral spherical ovaries (*arrows*) can be identified lateral of the uterine corpus in the ovarian fossa. Numerous uniformly sized follicles are found within the ovaries in this case of PCO, which was surgically verified

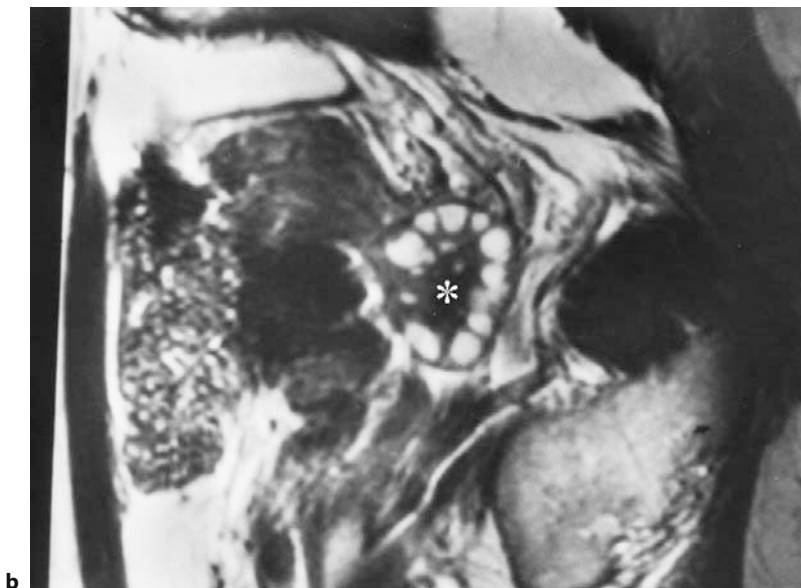
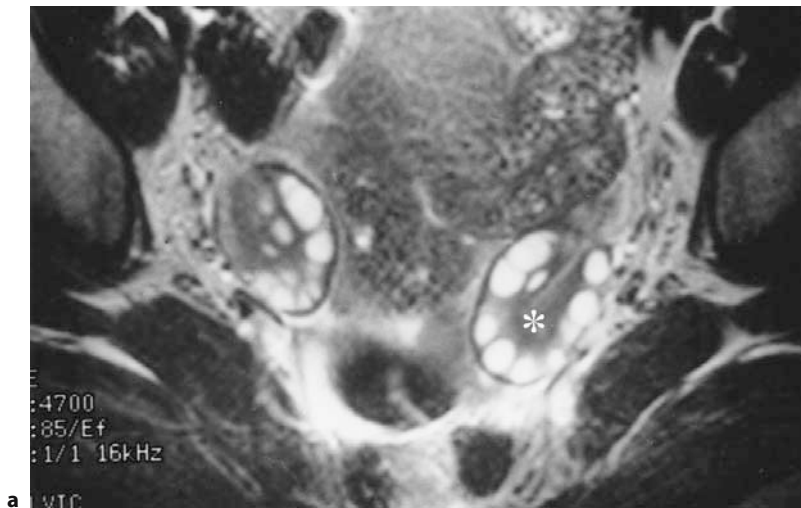


Fig. 9.24a,b. Polycystic ovaries in MRI. Transaxial T2-weighted images (a) and parasagittal T2 WI (b) in a patient with Stein-Leventhal syndrome. Bilateral spherical ovaries are demonstrated showing numerous small follicles of uniform size. The latter are located in the periphery of the ovary and surround the ovarian stroma (*asterisk*), which typically is of very low signal intensity on T2-weighted images in PCO

### 9.5.1.5.2

#### **Differential Diagnosis**

Multifollicular ovaries are found in mid to late puberty as a normal finding. Multifollicular ovaries may also result from hyperprolactinemia, hypothalamic anovulation, and weight-related amenorrhea. They may be differentiated from PCO by fewer cysts, the different size of follicles, lack of stromal hypertrophy, and the distribution of the often larger follicles throughout the ovary. In contrast to PCO, the ovaries resume normal appearance after treatment.

## 9.5.2

### **Benign Neoplastic Lesions of the Ovaries**

Benign ovarian neoplasm account for 80% of all tumors involving the ovaries. Although there is large spectrum of benign ovarian neoplasm, the vast majority are encompassed by only a few different histologic types. It is a matter of debate whether cystadenomas or teratomas are most frequent. In a large series cystic teratomas accounted for the majority of benign lesions (58%) followed by serous cystadenomas (25%) and mucinous cystadenomas (12%), benign stromal tumors (fibromas/fibrothecomas) (4%), and Brenner tumors (1%) [67].

#### 9.5.2.1

##### **Cystadenoma**

Cystadenomas account for 37%-50% of benign ovarian tumors in the reproductive age. Their frequency tends to increase with age, and after menopause, cystadenomas account for up to 80% of the benign ovarian tumors [1]. Cystadenomas are thin-walled unilocular or multilocular cystic lesions filled with serous mucinous, and sometimes hemorrhagic contents. Papillary projections within the cyst walls may be rarely found, but they should principally raise the suspicion of a borderline malignancy [68, 69]. The two types serous and mucinous cystadenomas differ in pathology, prognosis, and disease course.

Serous cystadenomas account for up to 40% of all benign ovarian neoplasms. They show a peak incidence in the fourth and fifth decades and are in up to 20% bilateral. Mucinous cystadenomas account for 20%-25% of all benign ovarian neoplasms, and are bilateral in only 2%-3% of cases. Both are cystic lesions filled with water-like or

higher proteinaceous contents. Calcified psammoma bodies are a typical feature of serous cystadenomas. Mucinous cystadenomas tend to be filled with sticky gelatinous fluid. They tend to be larger at the time of presentation. In contrast to serous cystadenomas, mucinous cystadenomas are typically multilocular with different contents of the loculi (Fig. 9.25) [1]. These loculi are small and multiple and separated by thin septations. Rupture of a mucinous cystadenoma can result in pseudomyxoma peritonei.

#### 9.5.2.1.1

##### **Imaging Findings**

Although an overlap exists, imaging features may aid in the differentiation of serous from mucinous cystadenomas [1]. Cystadenomas are well-circumscribed cystic tumors with enhancing thin walls and – if present – internal septations on CT and MRI (Fig. 9.25). The wall and septa are regular and thin (<3 mm) (Fig. 9.26). Papillary projections are rarely found in benign cystadenomas, and tend to be small (Fig. 9.1) [68].

The cystic loculi of serous cystadenomas display signal of simple fluid and tend to be low in signal on T1 and high on T2-weighted images (Fig. 9.11). In contrast, mucinous cystadenomas have often various signal intensities depending on the contents within the different loculi, which varies from watery to proteinaceous to hemorrhagic. The sticky gelatinous contents or mucin in mucinous cystadenomas display SI intensity higher than water on T2 and lower SI on T2-weighted images relative to serous fluid. When hemorrhage is present, blood products may be identified on MRI. The loculi of mucinous cystadenomas are often small and multiple. Multiple loculi with different contents within one lesion is a typical finding of mucinous cystadenomas. Rarely, they can manifest as a simple cyst.

Mucinous cystadenomas tend to be multilocular and larger at the time of presentation than serous cystadenomas. They present with a mean size of 10 cm, but may be as large as 30 cm [1].

#### 9.5.2.1.2

##### **Differential Diagnosis**

Serous and mucinous cystadenomas may display similar imaging findings in CT and MRI. If papillary projections are found in cystadenomas, they tend to be fewer and smaller than in borderline

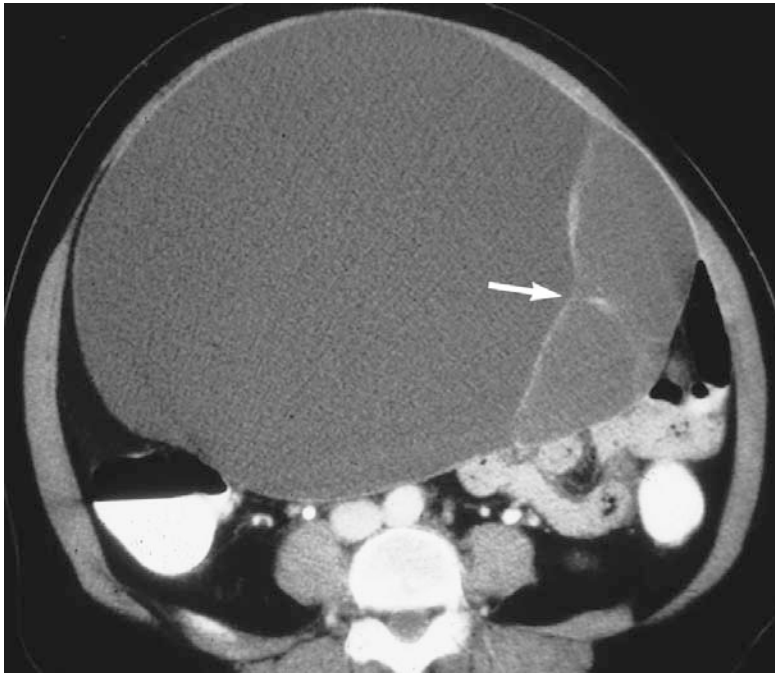


**Fig. 9.25.** Mucinous cystadenoma in CT. At the level of L5, a cystic ovarian lesion extending to the upper abdomen and measuring 25 cm in diameter is demonstrated. It bulges the abdominal wall and displaces bowel loops posteriorly. It displays multiple thin septations (*arrow*). Loculi in the left periphery display attenuation values which are higher than water. The large lesion size and different densities of the loculi are findings suggesting the diagnosis of a mucinous cystadenoma

tumors [68]. The presence of a mural nodule or focal wall thickening are signs highly indicative of malignancy. Microscopic foci of cystadenocarcinoma, which may arise in serous cystadenomas, will invariably be missed on imaging. Endometriomas may resemble mucinous cystadenomas, especially when they are complicated by hemorrhage. Low SI shading on the T2-weighted images is only found in endometrioma [54]. Furthermore, the walls in endometriomas tend to be thicker and irregular, and endometrioma usually are smaller than 10 cm. Hydrosalpinx can also display as a multiloculated uni- or bilateral adnexal lesion. In contrast to cystadenomas, the loculi communicate and incomplete septa are found. Furthermore, their origin from the tubal angle may enable the correct differential diagnosis.

#### 9.5.2.2 Cystadenofibroma

Cystadenofibromas account for 1.7% of ovarian tumors. They are benign serous ovarian tumors that display as cystic tumors with variable amounts of fibrous stroma. They can also be purely cystic with small foci of stroma detected microscopically. The margin tends to be well defined and smooth. Endocrine activity is not found.

#### 9.5.2.2.1 Imaging Features

The imaging features are nonspecific and may be similar to malignant tumors or borderline tumors. Variable amounts of fibrous stroma in ovarian cystadenofibromas produces imaging features that vary from purely cystic to a complex cystic tumor with one or more solid components (Fig. 9.27). In one series of 32 ovarian cystadenofibromas, 50% displayed as multiloculated masses identical to cystadenomas. The other half were complex cystic tumors with one or more solid components and smooth thickened septa [70].

#### 9.5.2.3 Benign Teratoma

Teratomas are the most common ovarian neoplasm in women under 45 years of age, and account for up to 70% of tumors in females less than 19 years of age [67]. Ovarian teratomas derive from germ cells and are classified into three main categories, among which the mature cystic teratomas account for 99%. Less common types of mature teratomas are the monodermal teratomas, which include the struma ovarii and carcinoid tumors. It is typical for monodermal teratomas not to be cystic but contain

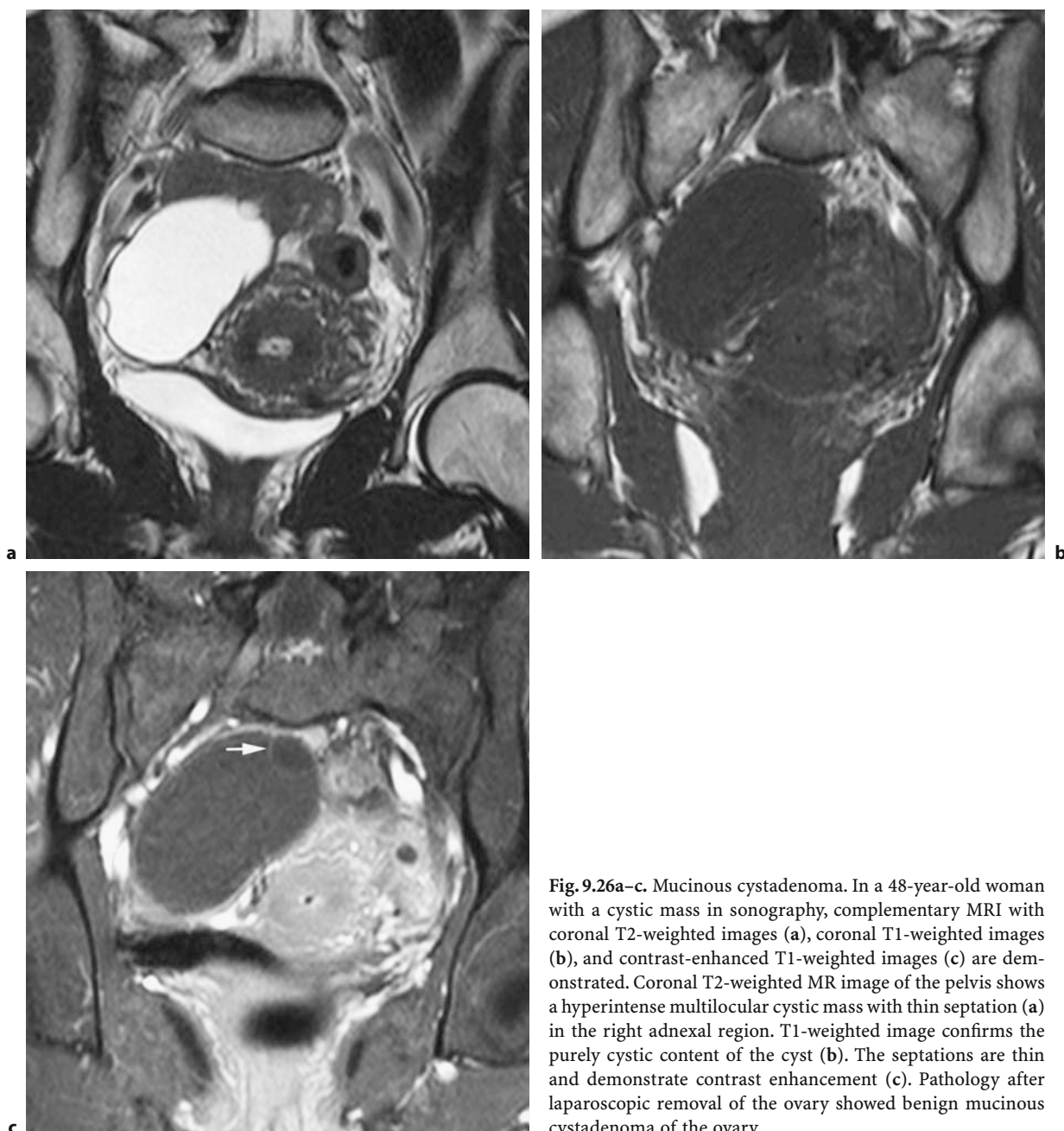


**Fig. 9.26a–c.** Mucinous cystadenoma. In a 48-year-old woman with a cystic mass in sonography, complementary MRI with coronal T2-weighted images (a), coronal T1-weighted images (b), and contrast-enhanced T1-weighted images (c) are demonstrated. Coronal T2-weighted MR image of the pelvis shows a hyperintense multilocular cystic mass with thin septation (a) in the right adnexal region. T1-weighted image confirms the purely cystic content of the cyst (b). The septations are thin and demonstrate contrast enhancement (c). Pathology after laparoscopic removal of the ovary showed benign mucinous cystadenoma of the ovary

primarily solid structures. Cystic teratomas typically contain lipid material consisting of sebaceous fluid within the cyst cavity or adipose tissue within the cyst wall or the dermoid plug [71].

#### 9.5.2.3.1

##### **Dermoid Cysts**

Dermoid cysts or mature cystic teratomas are composed of mature tissue from at least two of the three

germ cell layers: ectoderm, mesoderm, and endoderm. They are typically unilateral lesions, with only 10%-15% of dermoids found in both ovaries.

In the vast majority (88%), dermoid cysts are unilocular cystic lesions filled with sebaceous material. A protuberance, the Rokitansky nodule, or dermoid plug, projects into the cavity and is the hallmark of dermoids (Fig. 9.17). It contains a variety of tissues, often including fat and calcifications, which represent teeth or abortive bone. Fat is detected in over 90%,

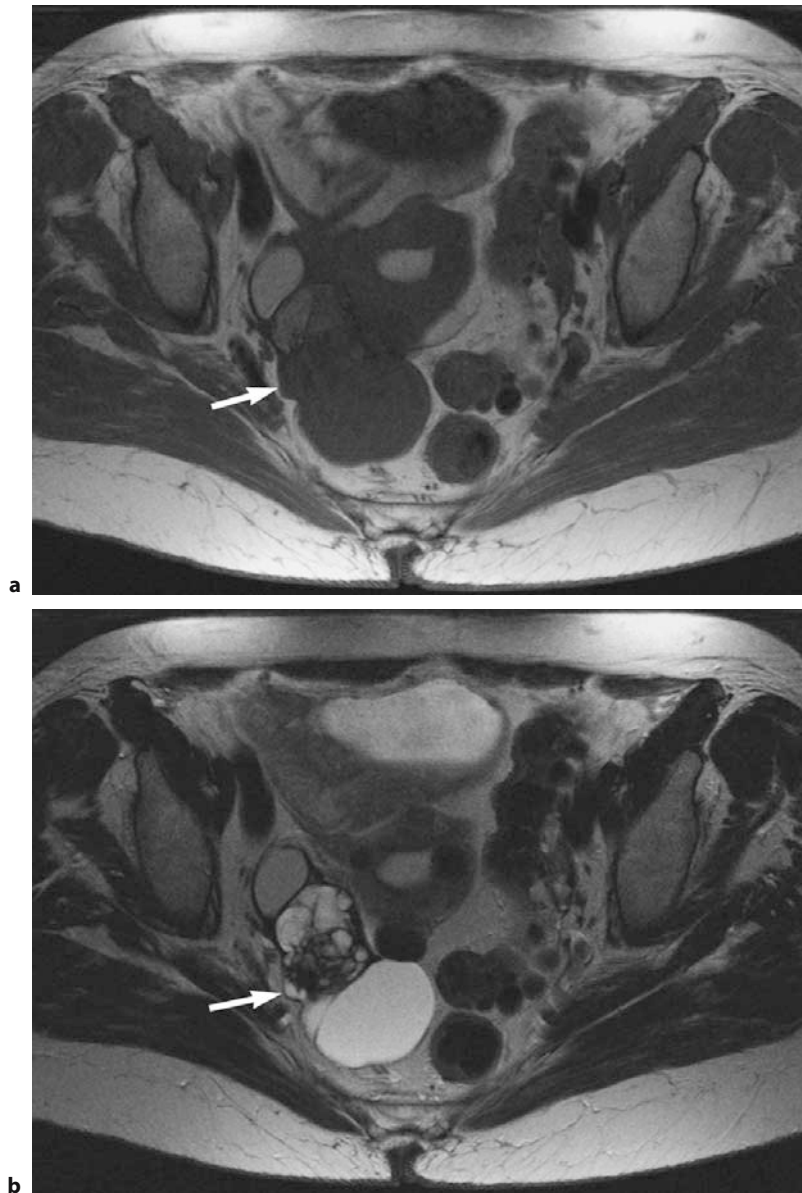


**Fig. 9.27a,b.** Cystadenofibroma. Transaxial T1 (a) and T2-weighted images (b). In a 77-year-old female, a cystic adnexal mass showing an increase in size in a follow-up underwent preoperative MRI. A multiseptate cystic right adnexal lesion (arrow) with multiple hemorrhagic-proteinaceous loculi displaying high SI on the T1-weighted images (a) is demonstrated. It displays irregular septa of very low SI on T2-weighted images (b). The uterus is enlarged due to fibroids; the uterine cavity is widened by hematometra

teeth in 31% and calcifications in the wall in 56% [72].

A minority of dermoid cysts will demonstrate no fat or only small foci of fat within the wall or the Rokitansky nodule (Fig. 9.28) [73]. YAMASHITA et al. reported that 15% of mature teratomas did not show fat within the cystic cavity. Approximately half of these cases displayed small amounts of fat within the wall of the dermoid or the dermoid plug. In 8% of benign teratomas, no fat could be detected [73].

Dermoids are usually asymptomatic and tend to grow slowly. This is why some gynecologists advo-

cate surgery in lesions larger than 6 cm in size [74]. Complications encountered with dermoid cysts are malignant degeneration and rupture, and with up to 16% torsion [75]. Malignant degeneration occurs in up to 2% and is usually found in the sixth to seventh decade; it is extremely rare and arises from the dermoid plug. The risk of malignancy is associated with large size (>10 cm) and postmenopausal age [76]. Rupture of a dermoid can cause acute abdomen due to granulomatous peritonitis caused by leakage of the fatty contents. Rarely, giant dermoids are found occupying the pelvis and abdomen.

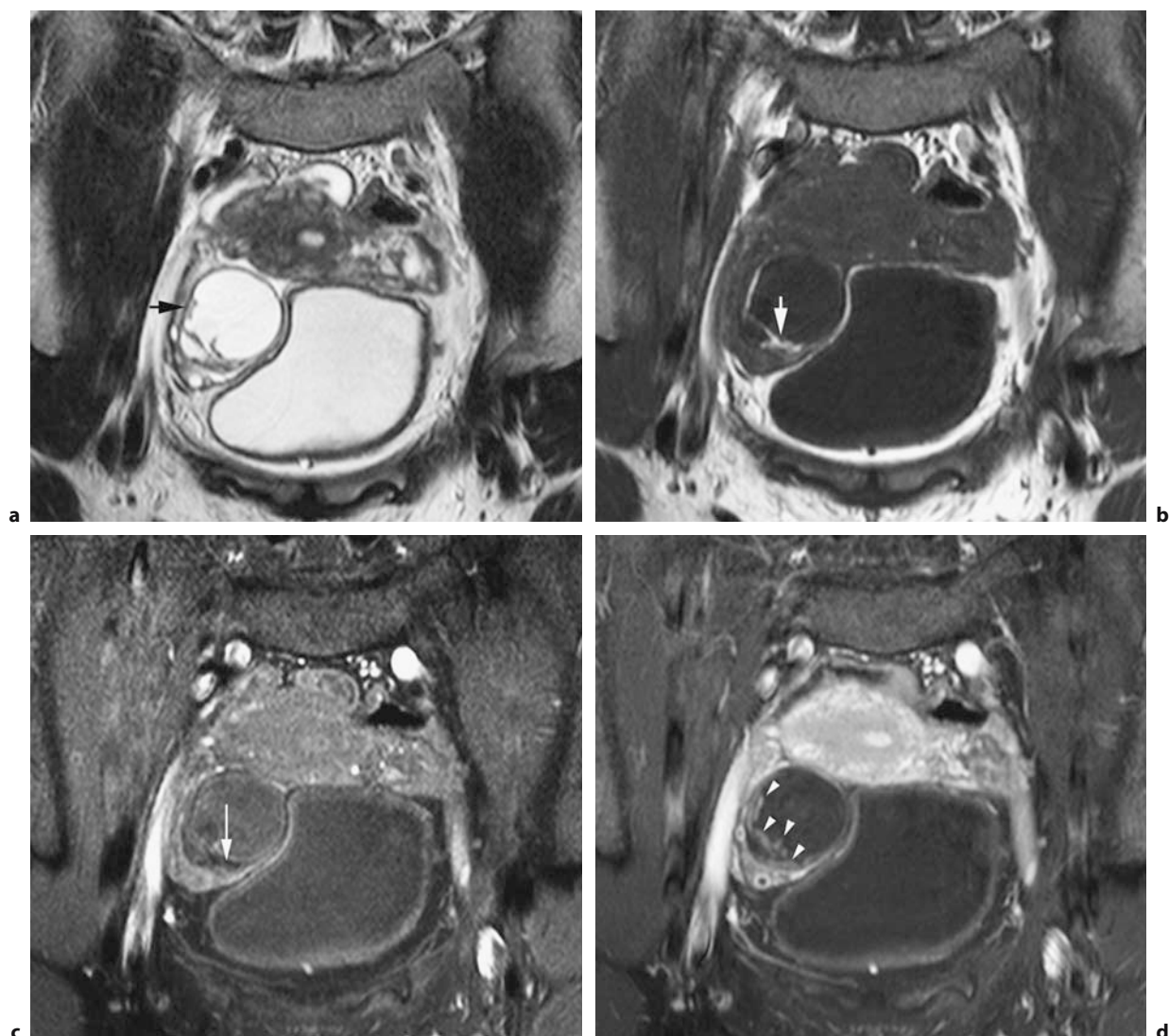


**Fig. 9.28a–d.** Dermoid with little fat. MRI was performed for further characterization of a sonographically suspicious cystic and solid mass in a 31-year-old woman. Coronal T2-weighted images (a), T1-weighted images (b), T1-weighted images with FS (c), contrast-enhanced T1-weighted images with FS (d). A multilocular mass with irregular wall thickening (arrow) (a) arising from the right adnexa is demonstrated. Coronal native T1-weighted image (b) confirms the cystic nature of the mass. A linear hyperintense portion is located at the lower part of the cyst (white arrow). The corresponding coronal fat-suppressed T1-weighted image (c) shows vanishing of the hyperintense linear part confirming the presence of a small amount of fat in the linear hypointense lower portion of the cyst (white arrow). The contrast-enhanced fat-suppressed T1-weighted image (d) shows enhancement of an irregular wall and septa (arrowheads) corresponding to the Rokitansky nodule of a dermoid cyst with little fat. Contrast enhancement of the mural protrusion of a mature cystic teratoma can be mistaken for ovarian cancer

### Imaging Findings

Sonographic assessment of dermoid cysts is often limited by its variety of appearance.

At CT and MRI, however, the diagnosis of fat within a cystic mass is pathognomonic for a mature cystic teratoma [73]. The fatty elements display characteristic low CT attenuation (–20 to –120 HU)

(Fig. 9.29). Another typical feature on CT is the presence of calcifications within the cyst wall or the dermoid plug.

The typical MRI findings include a round or oval, sharply delineated lesion with high SI on T1-weighted images, and loss of signal on the fat-saturated T1-weighted images, representing fat (Fig. 9.30). This fatty content may display a broad spectrum of



**Fig. 9.29.** Dermoid torsion in CT. Non-contrast transaxial CT in a 37-year-old female who presented with acute pelvic pain. A well-demarcated left adnexal lesion with fatty attenuation values (*asterisk*) is located adjacent to the uterus. Linear calcifications are found at its medial wall. An area of higher density within the fatty tissue correlated with floating hair in the macroscopic specimen. The homogenous wall thickening (*arrow*) is caused by edema due to torsion of the dermoid

appearance, including a fat-filled cavity, foci of fat within the lesion or its wall, and a fat–fluid interface often representing a floating mass of hair.

On T2-weighted images, the signal may be variable, but it tends to be similar to subcutaneous fat. Furthermore, chemical shift artifacts in the frequency-encoding direction can be observed, which confirms the presence of fat and differentiates it from hemorrhage [77]. Calcification in the wall of cystic teratomas and in the dermoid plug will often be missed on MRI due to the low SI on T1- and T2-weighted images.

In a patient with acute abdomen and a dermoid, the presence of sebaceous fluid floating in the peritoneal cavity can suggest rupture [75].

### Differential Diagnosis

Although hemorrhagic lesions including endometrioma, hemorrhagic cysts, and neoplasm may appear similar on the T1-weighted images and T2-weighted images, fat-suppressed or chemical shift images are most reliable for the differentiation of fat from hemorrhage [78].

When no or only small amounts of fat are present (8%), dermoids are not distinguishable from benign cystic ovarian tumors or ovarian cancer (Fig. 9.28) [75].

Capsule perforation often arising from the dermoid plug is a sign for malignant transformation of a mature teratoma [79]. The rare liposarcoma or immature teratoma may contain fat and thus may be indiscernible from a dermoid. Immature teratomas, however, are extremely rare, and occur in the first two decades of life. They may occur in association with an ipsilateral dermoid in 26%, and a contralateral dermoid in 10%. However, at the time of presentation they are usually very large, are predominantly solid or

cystic and solid, and contain only few foci of fat [80]. Collision tumors of the ovary consisting of a mature cystic teratoma and a mucinous cystadenoma show a multiloculated cystic mass with an area of pure fat (Fig. 9.31) [81].

### 9.5.2.3.2

#### Monodermal Teratoma

Monodermal teratomas are composed predominantly or solely of one tissue type. They include struma ovarii, ovarian carcinoid tumors, and tumors with neural differentiation.

Struma ovarii is the most common type, and accounts for 3% of all mature teratomas. It consists predominantly or solely of mature thyroid tissue. A mixed morphology with acini filled with thyroid colloid, hemorrhage, fibrosis, and necrosis is found. Rarely struma ovarii may produce thyrotoxicosis.

Carcinoid tumors are frequently associated with a mature cystic teratoma or a mucinous ovarian tumor. Unlike most cystic teratomas, they are predominantly found in postmenopausal women. The course is usually benign; rarely will metastases be found. Carcinoid syndrome is uncommon.

#### Imaging Findings

On CT and MRI, a struma ovarii displays as a heterogeneous complex mass (Fig. 9.13). They present as cystic lesions or with a multilocular appearance with loculi displaying high signal intensity on T1 and T2, some with low signal intensity on T1 and T2-weighted images on MR. Fat is not seen in struma ovarii [82].

Carcinoid tumors are solid tumors indistinguishable from solid ovarian malignancies.

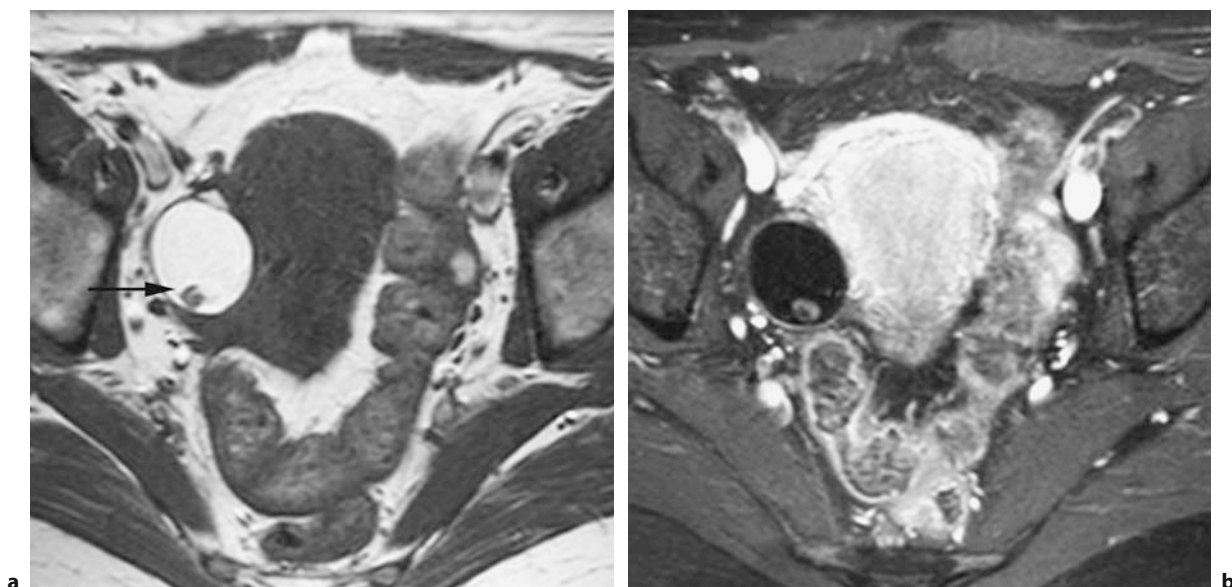


**Fig. 9.30a,b.** Typical findings of dermoid in MRI. A 44-year-old woman complaining about irregular menstrual cycle and a suspicious adnexal mass at transvaginal ultrasound. Axial T1-weighted images (a) and T1-weighted images contrast-enhanced image with fat suppression (b) at the acetabular level. The cystic structure of the right ovary demonstrates hyperintense contents with a round nodule in the lower part of the cyst (*arrow*) (a). The hypointense content after fat suppression (b) confirms the fatty nature of the cyst. At pathology, the round nodule corresponded to a hair ball within a mature cystic teratoma

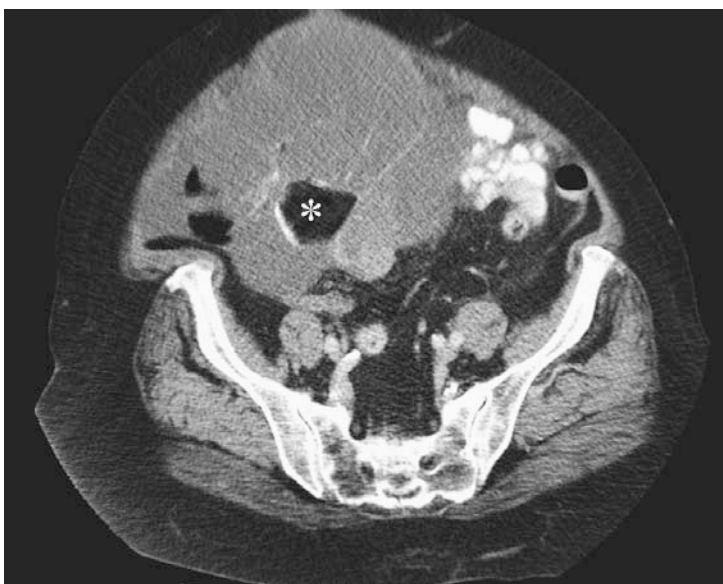


**Fig. 9.31.** Collision tumor of the ovary. CT at the level of the mid pelvis in a 65-year-old woman with sonographically suspected ovarian cancer. A cystic right adnexal mass is demonstrated showing multiple thin septations and a 3-cm lesion with fat density and mural calcifications (*asterisk*). Pathologically, a collision tumor composed of a benign mucinous cystadenoma and a benign dermoid was diagnosed

#### 9.5.2.4 Benign Sex Cord Stromal Tumors

Sex cord stromal tumors include neoplasms that are composed of granulosa cells, theca cells, and their luteinized derivatives, including Sertoli cells, Leydig cells, and fibroblasts of gonadal stromal origin [37].

Tumors of the thecoma-fibroma subgroup are characterized by fibrous components and include fibroma, fibrothecoma, cystadenofibroma, and Brenner tumors. They account for the vast majority of the sex cord stromal tumors and are benign, except for Brenner tumors, which may rarely be malignant.

## 9.5.2.4.1

**Fibroma and Fibrothecoma**

Fibromas and fibrothecomas are solid ovarian tumors accounting for 3%-4% of all ovarian tumors and 10% of solid adnexal masses. They are typically unilateral (90%), and occur in peri- and postmenopausal age women.

Fibromas are composed mostly of fibroblasts and spindle cells and abundant collagen contents. Fibromas are not hormonally active. Fifteen percent of fibromas are associated with ascites (Fig. 9.32), and in 1% pleural fluid is also found [83]. This triad of an ovarian fibroma, ascites and pleural effusion constitutes the benign Meigs syndrome, which can be associated with elevated Ca-125 levels [84]. In basal cell nevus syndrome, numerous basal cell carcinomas are associated with abnormalities of bones, eyes, brain, and tumors, including ovarian bilateral fibromas [85].

Thecomas are composed of thecal cells with abundant and varying amounts of fibrosis, and rarely contain calcifications. Unlike fibromas, 60% of thecomas

have estrogenic activity and may present with uterine bleeding. Furthermore, in more than 20%, endometrial carcinomas may be present concomitantly [85].

**Imaging Findings**

Small fibromas and fibrothecomas are solid tumors with imaging features similar to nondegenerative uterine leiomyomas on CT and MRI (Fig. 9.33). They display intermediate to low SI on T1-weighted images and typically very low SI or low SI with intermediate SI on the T2-weighted images on MRI (Fig. 9.32). Large lesions may have an inhomogenous architecture with high signal intensity foci within the low signal intensity lesion, representing edema or cystic degeneration [21]. Furthermore, especially in larger lesions, dense amorphous calcifications may be seen, which are easily detected on CT. On MRI, calcifications are typically not appreciated because of their low SI on the T2-weighted images. Fibromas and fibrothecomas tend to show mild or delayed gadolinium enhancement (Fig. 9.32) [86]. Ascites may be

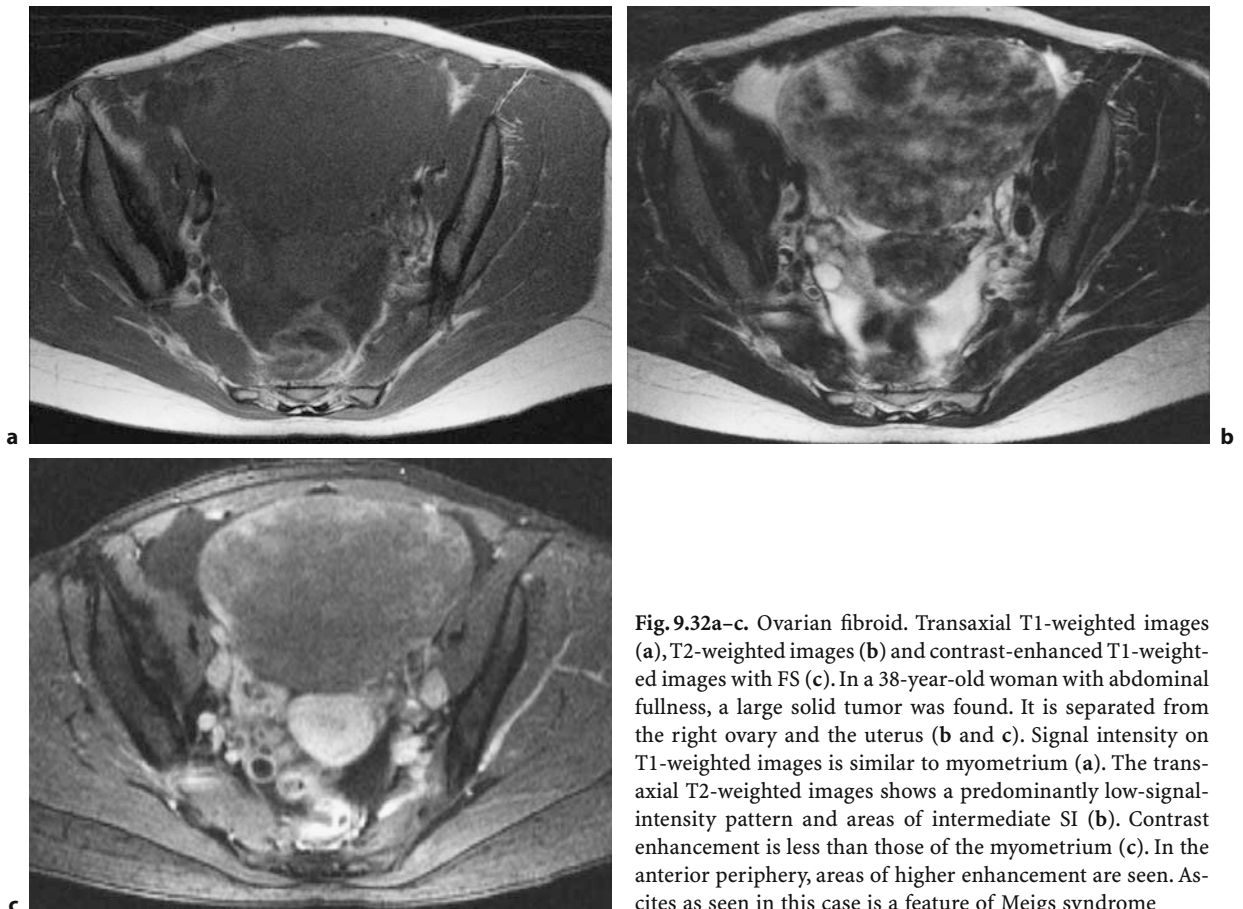


**Fig. 9.32a-c.** Ovarian fibroid. Transaxial T1-weighted images (a), T2-weighted images (b) and contrast-enhanced T1-weighted images with FS (c). In a 38-year-old woman with abdominal fullness, a large solid tumor was found. It is separated from the right ovary and the uterus (b and c). Signal intensity on T1-weighted images is similar to myometrium (a). The transaxial T2-weighted images shows a predominantly low-signal-intensity pattern and areas of intermediate SI (b). Contrast enhancement is less than those of the myometrium (c). In the anterior periphery, areas of higher enhancement are seen. Ascites as seen in this case is a feature of Meigs syndrome

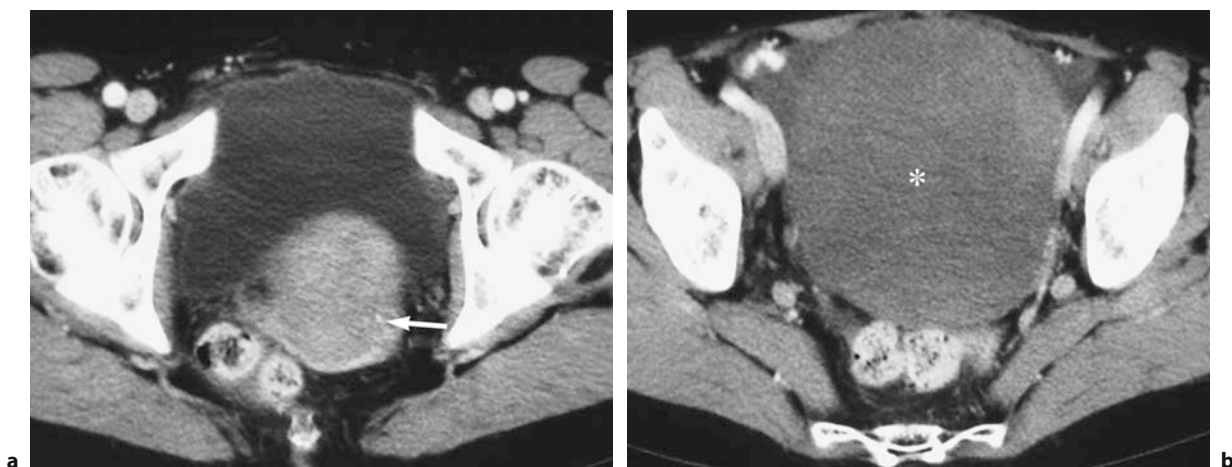


**Fig. 9.33a,b.** Ovarian fibroma in CT. Transaxial pelvic CT at the uterine level (a) and above (b) in a 55-year-old woman with abdominal fullness. A large lesion (*asterisk*) is found in the mid pelvis above the level of the uterus and bladder (b). It is well demarcated and displays a slightly inhomogeneous solid structure. Contrast enhancement is distinctly less than that of the myometrium (*arrow*). No calcifications were found throughout the lesion. Minimal ascites was seen. Histopathology revealed a 9-cm fibroid of the left ovary

present and even large amounts are no sign of malignancy.

#### 9.5.2.4.2

##### **Brenner Tumors**

Brenner tumors present rare ovarian tumors that occur at a mean age of 50 years. Brenner tumors constitute 1%–3% of ovarian tumors. They are mostly benign, with less than 2% demonstrating borderline or malignant transformation. They are typically small, solid, unilateral ovarian tumors, with 60% of these tumors found under 2 cm in size. Extensive calcification may be observed. The vast majority is discovered incidentally in pathologic specimen of the adnexa. Brenner tumors rarely produce estrogen, and then they may be associated with endometrial thickening [87]. If cystic components are found in Brenner tumors, they may be associated with cystadenomas [88]. Up to 20% of Brenner tumors are associated with mucinous cystadenomas or other epithelial neoplasm (Fig. 9.34).

##### **Imaging Findings**

The typical finding of a Brenner tumors is a small solid tumor that displays very low SI on the T2-weighted images [87]. Dense amorphous calcifications in a small solid ovarian tumor is a typical CT finding. In one series of eight Brenner tumors, the

mean size was 11.5 cm, and tumors displayed a mixed solid and cystic appearance in half of the cases, which mimicked ovarian cancer [87]. The combination of a multiseptate ovarian tumor with a solid part displaying extensive calcifications on CT or very low SI on MRI may suggest the diagnosis of a collision tumor of Brenner tumor and a cystic ovarian neoplasm, e.g., cystadenoma (Fig. 9.34).

#### 9.5.2.4.3

##### **Sclerosing Stromal Tumor of the Ovary**

Sclerosing stromal tumor of the ovary is a rare subtype of the sex cord stromal tumor type. It is a benign tumor and affects most commonly young girls and women younger than 30 years of age, which is much earlier than in the other stromal tumor types [89]. Macroscopically, these tumors have a capsule with peripheral edematous ovarian cortical stroma surrounding nodular highly vascular cellular components [89]. These tumors may have an estrogenic effect and rarely androgenic effects, which cause prolonged menstrual irregularities. Ascites may be rarely associated.

##### **Imaging Findings**

Sclerosing stromal cell tumors tend to be well encapsulated multiloculated cystic or heterogenous ovarian lesions (Fig. 9.35). On T1 and T2-weighted images, a

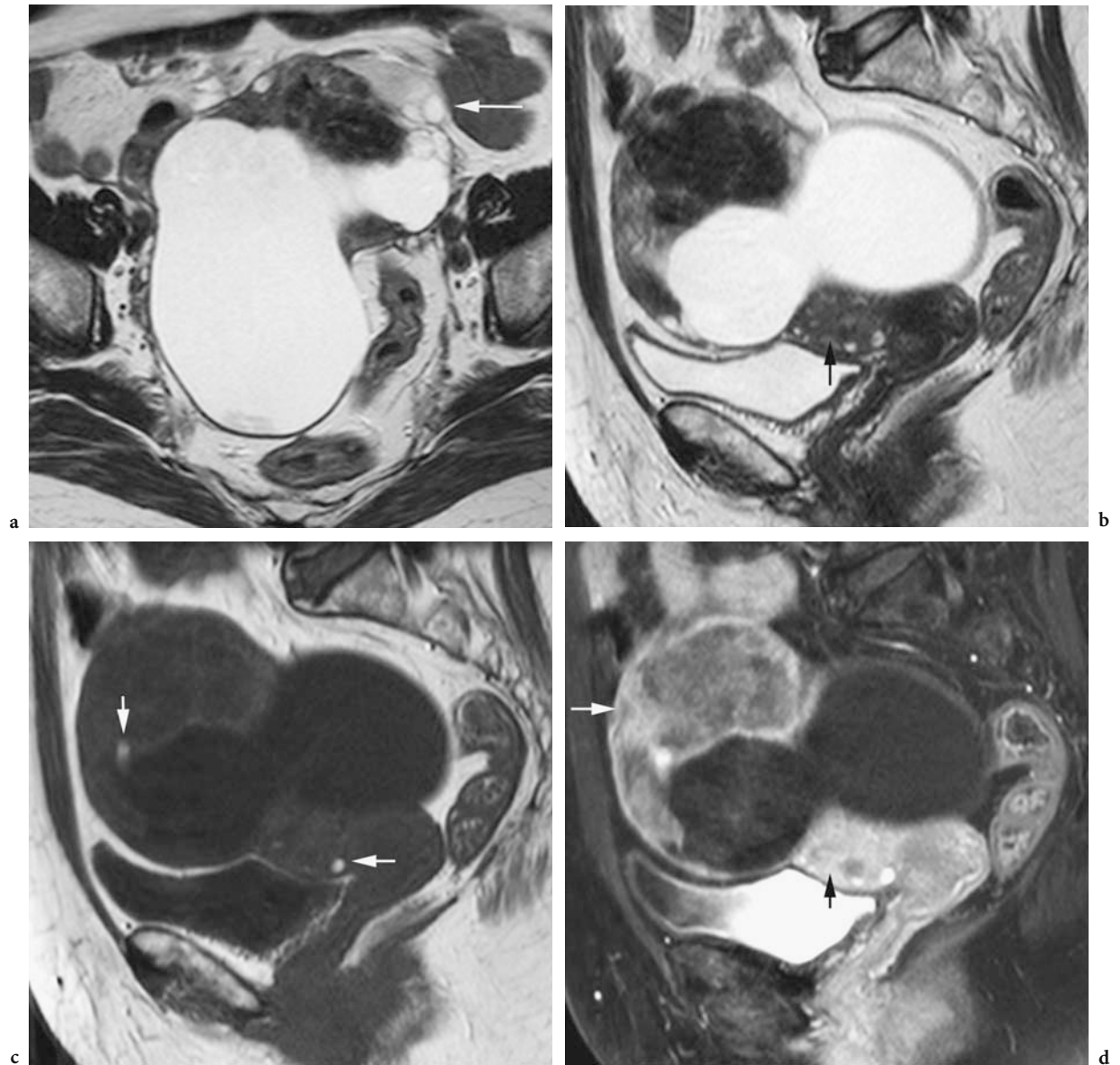


**Fig. 9.34a–d.** Large Brenner tumors with mucinous portion. A 75-year-old woman presenting with a large suspicious pelvic mass at ultrasound and moderate increase in Ca125 level. Axial T2-weighted images (a), sagittal T2-weighted images (b), Sagittal T1-weighted images (c), Sagittal T1-weighted images with FS. (d) A cystic mass with a solid hypointense anterior portion is demonstrated (a). Ovarian parenchyma with two follicles is seen at the left anterior side (arrow). The small uterus (arrow) is identified below the left ovarian mass (b). The interface between the cystic and solid portion of the mass is regular. Sagittal T1-weighted images (c) shows absent blood within the cyst except for two blood vessels seen within the solid portion of the mass and the anterior myometrium (arrows). At the same level as b and c contrast-enhanced T1-weighted image with fat suppression (d) shows heterogeneous decreased contrast enhancement of the solid portion of the cyst (white arrow) compared to the strongly enhancing myometrium (black arrow). Histology after hysterectomy and bilateral oophorectomy diagnosed a benign Brenner tumor of the left ovary with an associated benign mucinous portion

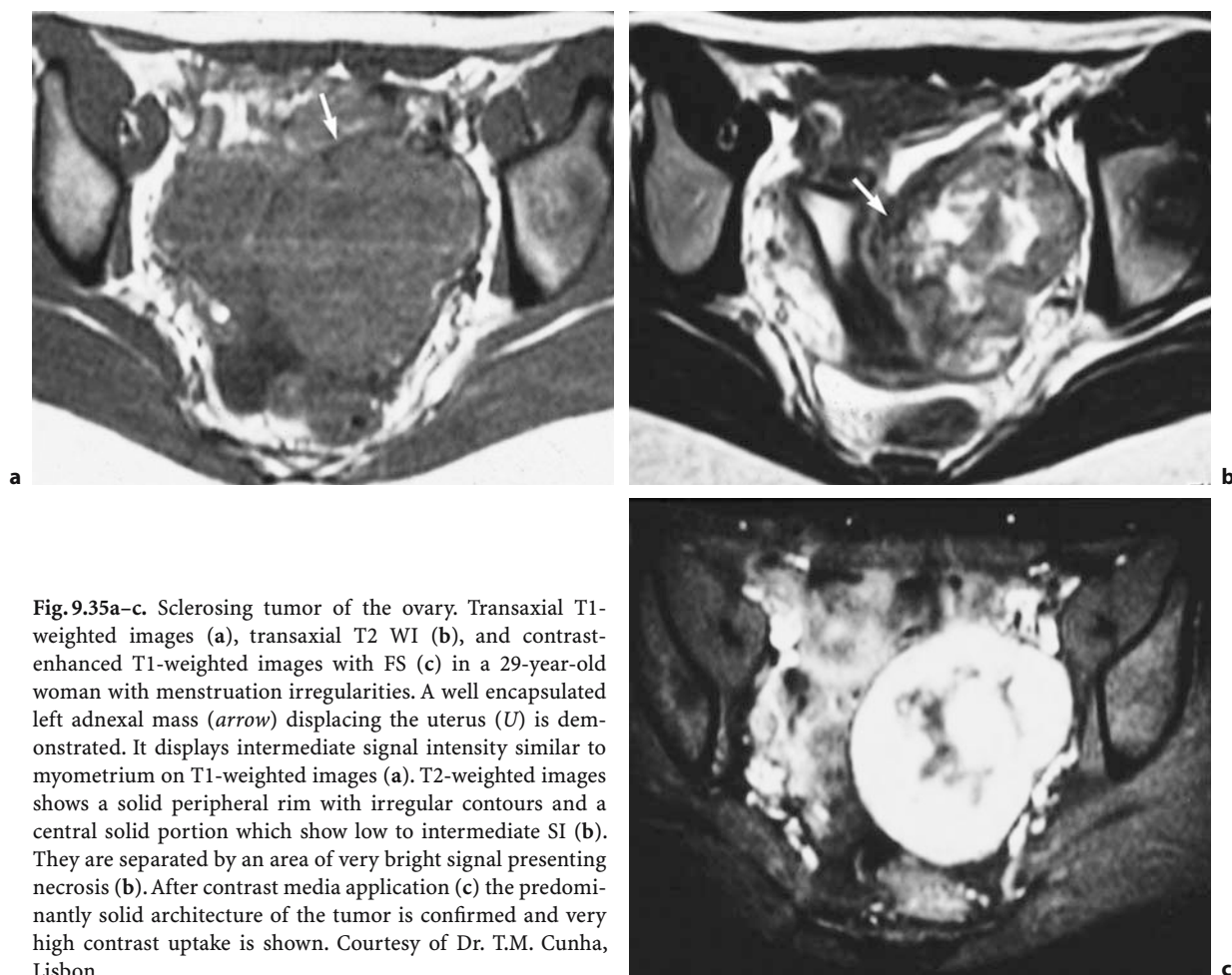


**Fig. 9.35a–c.** Sclerosing tumor of the ovary. Transaxial T1-weighted images (a), transaxial T2 WI (b), and contrast-enhanced T1-weighted images with FS (c) in a 29-year-old woman with menstruation irregularities. A well encapsulated left adnexal mass (*arrow*) displacing the uterus (*U*) is demonstrated. It displays intermediate signal intensity similar to myometrium on T1-weighted images (a). T2-weighted images shows a solid peripheral rim with irregular contours and a central solid portion which show low to intermediate SI (b). They are separated by an area of very bright signal presenting necrosis (b). After contrast media application (c) the predominantly solid architecture of the tumor is confirmed and very high contrast uptake is shown. Courtesy of Dr. T.M. Cunha, Lisbon

thin low-intensity rim representing a capsule is seen. On T2-weighted images, in the periphery an irregular low-signal-intensity rim is found adjacent to a very bright more central portion, which has a nodular appearance. On dynamic MRI, lack of enhancement of the outermost part and distinct early peripheral enhancement with centripetal progression on delayed images has been described [89].

### Differential Diagnosis

The solid morphology and the signal characteristics of fibromas and fibrothecomas are fairly characteristic. Pedunculated uterine fibroids and fibroids of the broad ligaments can display similar imaging characteristics. The latter can only be differentiated from ovarian fibromas or fibrothecomas when they are separated from the ovary. Subserosal pedunculated fibroids can be discrimi-

nated by the bridging vascular sign. Unilateral or bilateral ovarian leiomyomas are extremely rare, and cannot be reliably differentiated by imaging. High-contrast media uptake in such a lesion might suggest ovarian leiomyoma [90]. Fibromas and fibrothecomas with large central necrotic areas cannot be reliably differentiated from malignant solid ovarian masses, especially Krukenberg tumors. In contrast to the majority of ovarian tumors, only little or delayed contrast enhancement is observed in ovarian stromal tumors. Dense calcifications in CT support also the diagnosis of stromal tumors. Small calcified solid tumors favor the diagnosis of Brenner tumors. A multicystic tumor with focal very dense calcifications, which is only reliably appreciated on CT, may suggest the diagnosis of Brenner tumor and cystadenoma. In contrast, calcifications in ovarian cancer tend to be small punctuate foci, so-called Psammoma bodies.

Sclerosing stromal cell tumors seem to have a unique distinct centripetal contrast media uptake. Morphologically, they may resemble Krukenberg tumors or dysgerminomas.

## References

- Jung SE, Lee JM, Rha SE et al (2002) CT and MRI of ovarian tumors with emphasis on the differential diagnosis. *Radiographics* 22:1305–1325
- Sala EJ, Atri M (2003) MRI of benign adnexal disease. *Top Magn Reson Imaging* 14:305–328
- Yamashita Y, Tang Y, Abe Y, Mitsuzaki K, Takahashi M (1998) Comparison of ultrafast half-Fourier single-shot turbo spin-echo sequence with turbo spin-echo sequences for T2-weighted imaging of the female pelvis. *J Magn Reson Imaging* 8:1207–1212
- Niitsu M, Tanaka YO, Anno I, Itai Y (1997) Multishot echo-planar MR imaging of the female pelvis: comparison with fast spin-echo MR imaging in an initial clinical trial. *AJR Am J Roentgenol* 168:651–655
- Maubon A, Berger V, Aubas P et al (1999) Abdominal and pelvic segmented T1-weighted echo-planar imaging and MRI. Comparison with T1-TSE and T2-UTSE sequences. *J Radiol* 80:291–296
- Yamashita Y, Harada M, Sawada T, Takahashi M, Miyazaki K, Okamura H. (1993) Normal uterus and FIGO stage I endometrial carcinoma: dynamic gadolinium-enhanced MR imaging. *Radiology* 186:495–501
- Hricak H, Chen M, Coakley FV et al (2000) Complex adnexal masses: detection and characterization with MRI: multivariate analysis. *Radiology* 214:39–46
- Wu TT, Coakley FV, Qayyum A et al (2004) Magnetic resonance imaging of ovarian cancer arising in endometriomas. *J Comput Assist Tomogr* 28:836–838
- Saksouk FA, Johnson SC (2004) Recognition of the ovarian origin of pelvic masses with CT. *Radiographics* 24: S133–S146
- Levine CD, Patel UJ, Ghanekar D (1997) Benign extraovarian mimicks of ovarian cancer: distinction with imaging studies. *Clin Imaging* 21:350–358
- Foshager MC, Hood LL, Walsh JW et al (1996) Masses simulating gynaecologic diseases at CT and MRI. *Radiographics* 16:1085–1099
- Lee JH, Jeong YK, Park JK et al (2003) Ovarian vascular pedicle sign revealing organ origin of mass lesion on helical CT. *AJR Am J Roentgenol* 181:131–137
- Kim JC, Kim SS, Park JY (2003) Bridging vascular sign in the MR diagnosis of exophytic uterine leiomyoma. *J Comput Assist Tomogr* 24:57–60
- Outwater EK, Siegelman ES, Chiowanich P et al (1988) Dilated fallopian tubes: MRI characteristics. *Radiology* 208:463–469
- Kobal B, Rakar S, Ribl M et al (1999) Pretreatment evaluation of adnexal tumors predicting ovarian cancer. *Int J Gynecol Cancer* 6:481–487
- Brown DL, Doubilet PM, Miller FH et al (1998) Benign and malignant ovarian masses: selection of most discriminating gray scale and Doppler sonographic features. *Radiology* 208:103–110
- Alcazar JL, Jurado M (1998) Using a logistic model to predict malignancy of adnexal masses based on menopausal status, ultrasound morphology, and color Doppler findings. *Gynecol Oncol* 69:146–150
- Kinkel K, Hricak H, Lu Y et al (2000) US characterization of ovarian masses: a meta-analysis. *Radiology* 217:803–811
- Buy JN, Ghossain MA, Hugol D et al (1996) Characterization of adnexal masses: combination of color Doppler and conventional sonography compared with spectral Doppler analysis alone and conventional sonography alone. *AJR Am J Roentgenol* 166:385–393
- Quinn SF, Erickson S, Black WC (1985) Cystic ovarian teratomas: the sonographic appearance of the dermoid plug. *Radiology* 155:477–478
- Bazot M, Ghossain MA, Buy JN et al (1993) Fibrothecomas of the ovary: CT and US findings. *J Comput Assist Tomogr* 17:754–759
- Atri M, Nazarnia S, Bret PM et al (1994) Endovaginal sonographic appearance of benign ovarian masses. *Radiographics* 14:747–760
- Ekici E, Soysal M, Kara S, Dogan M, Gokmen O (1996) The efficiency of ultrasonography in the diagnosis of dermoid cysts. *Zentralbl Gynakol* 118:136–141
- Patel MD, Feldstein VA, Chen DC et al (1999) Endometriomas: diagnostic performance of US. *Radiology* 210:739–745
- Brown DL, Frates MC, Muto MG, Welch WR (2004) Small echogenic foci in the ovaries: correlation with histologic findings. *J Ultrasound Med* 23:307–313
- Yamashita Y, Torashima M, Hatanaka Y et al (1995) Adnexal masses: accuracy of characterization with transvaginal US and precontrast and postcontrast MRI. *Radiology* 194:557–565
- Stevens SK, Hricak H, Stern JL (1991) Ovarian lesions: detection and characterization with gadolinium-enhanced MRI at 1.5 T. *Radiology* 181:481–488
- Sohaib SA, Sahdev A, Van Trappen P et al (2003) Characterization of adnexal lesions on MRI. *AJR Am J Roentgenol* 180:1297–1304
- Kawamoto S, Urban BA, Fishman EK (1999) CT of epithelial ovarian tumors. *Radiographics* 19:85–102
- Dorum A, Blom GP, Ekerhovd E et al (2005) Prevalence and histologic diagnosis of adnexal cysts in postmenopausal women: an autopsy study. *Am J Obstet Gynecol* 192:48–54
- Goldstein SR, Subramanyam B, Synder JR et al (1989) The postmenopausal cystic adnexal mass: the potential role of ultrasound in conservative management. *Obstet Gynecol* 73:8–10
- Rulin MC, Preston AI (1987) Adnexal masses in postmenopausal women. *Obstet Gynecol* 70:578–581
- Outwater EK, Wilson KM, Siegelman ES, Mitchell DG (1996) MRI of benign and malignant gynecologic disease: significance of fluid and peritoneal enhancement in the pelvis. *Radiology* 200:483–488
- Walkey MM, Friedman AC, Sohotra P et al (1988) CT manifestations of peritoneal carcinosis. *AJR Am J Roentgenol* 150:1035–1041
- Occhipinti KA (1999) CT and MRI of the ovary. In: Anderson JC (ed) *Gynecologic imaging*. Churchill Livingstone, London pp 345–359
- Tanaka YO, Tsunoda H, Kitagawa Y et al (2004) Functioning

- ovarian tumors: direct and indirect findings at MR imaging. *Radiographics* 24:147–166
37. Young RH, Scully RE (2002). Sex cord stromal, steroid cell, and other ovarian tumors. In: Kurman RJ (ed) *Blaustein's pathology of the female genital tract*. Springer Verlag, New York, pp 903–966
  38. Outwater EK, Wagner BJ, Nannion C et al (1998) Sex cord stromal and steroid cell tumors of the ovary. *Radiographics* 18:1523–1546
  39. Garcia-Villaneuva M, Figuerola NB, del Arbol LR et al (1990) Zollinger Ellison syndrome due to a borderline mucinous cystadenoma of the ovary. *Obstet Gynecol* 75:549–551
  40. Norris HJ, Jensen RD (1972) Relative frequency of ovarian neoplasm in children and adolescents. *Cancer* 30:713–719
  41. Laufer MR, Goldstein DP (2005) Ovarian cysts and neoplasm in infants, children, and adolescents. [www.uptodate.com](http://www.uptodate.com)
  42. Cass DL, Hawkins E, Brandt ML et al (2001) Surgery for ovarian masses in infants, children, and adolescents: 102 consecutive patients treated in a 15-year period. *J Pediatr Surg* 36:693–699
  43. Frisch LS, Copeland KC, Boepple PA (1992) Recurrent ovarian cysts in childhood: diagnosis of McCune-Albright syndrome by bone scan. *Pediatrics* 90:102–104
  44. Van Winter JT, Simmons PS, Podratz KC (1994) Surgically treated adnexal masses in infancy, childhood, and adolescence. *Am J Obstet Gynecol* 170:1780–1786
  45. Dorigo O, Berek JS (2005) Epidemiology, pathology, and clinical manifestations of ovarian germ cell tumors. [www.Uptodate.com](http://www.Uptodate.com)
  46. Jabra AA, Fishman EK, Taylor GA (1993) Primary ovarian tumors in the pediatric patient: CT evaluation. *Clin Imaging* 17:199–203
  47. Hermans RHM, Fisher DC, van der Putte HWHM et al (2003) Adnexal masses in pregnancy. *Onkologie* 26:167–172
  48. Sherard GB, Hodson CA, Williams HJ et al (2003) Adnexal masses and pregnancy: a 12-year experience. *Am J Obstet Gynecol* 189:358–362
  49. Nagayama M, Watanabe Y, Okumura A et al (2002) Fast MR imaging in obstetrics. *Radiographics* 22:363–380
  50. Birchard KR, Brown MA, Hyslop WB et al (2005) MRI of acute abdominal and pelvic pain in pregnant patients. *AJR Am J Roentgenol* 184:452–458
  51. Outwater EK, Mitchell DG (1996) Normal ovaries and functional cysts: MR appearance. *Radiology* 198:397–402
  52. Guerriero S, Ajossa S, Lai MP et al (2003) The diagnosis of functional ovarian cysts using transvaginal ultrasound combined with clinical parameters, CA 125 determinations, and color Doppler. *Eur J Obstet Gynecol Reprod Biol* 110:83–88
  53. Christensen JT, Boldsen JL, Westergaard JG (2002) Functional ovarian cysts in premenopausal and gynecologically healthy women. *Contraception* 66:153–157
  54. Togashi K, Nishimura K, Kimura I (1991) Endometrial cysts: diagnosis with MRI. *Radiology* 180:73–78
  55. Kier R (1992) Nonovarian gynaecologic cysts: MR imaging findings. *AJR* 158:1265–1269
  56. Kim JS, Lee HJ, Woo SK et al (1997) Peritoneal inclusion cysts and their relationship to the ovaries: evaluation with sonography. *Radiology* 204:481–484
  57. Honore LH, O'Hara KE (1980) Serous papillary neoplasms arising in paramesonephric paraovarian cysts: a report of 8 cases. *Acta Obstet Gynecol Scand* 59:525–528
  58. Kishimoto K, Ito K, Awaya H et al (2002) Paraovarian cysts: MR imaging features. *Abdom Imaging* 27:685–689
  59. Kurachi H, Marakami T, Nakamura H et al (1993) Imaging of peritoneal pseudocysts: value of MRI compared with sonography and CT. *AJR Am J Roentgenol* 161:589–591
  60. Clement PB (2002) Non-neoplastic lesions of the ovary. In: Kurman RJ (ed) *Blaustein's pathology of the female genital tract*. Springer Verlag, New York, pp 675–728
  61. Lakhani K, Seifalian AM, Atiomo WU et al (2002) Polycystic ovaries. *BJR* 75:9–16
  62. Polson DW, Adams J, Wadsworth J et al (1988) Polycystic ovaries: a common finding in normal women. *Lancet* 1:870–872
  63. Ginsburg J, Havard CWM (1976) Polycystic ovary syndrome. *Br Med J* 2:737–740
  64. Park SJ, Lim JW, Ko YT et al (2004) Diagnosis of pelvic congestion syndrome using transabdominal and transvaginal sonography. *AJR* 182:683–688
  65. Kyei-Mensah A, Zaidi J, Campbell S (1996) Ultrasound diagnosis of polycystic ovary syndrome. *Baillieres Clin Endocrinol Metabol* 10:249–262
  66. Mitchell DG, Geftter WB, Spritzer CE et al (1986) Polycystic ovaries: MR imaging. *Radiology* 160:425–429
  67. Koonings PP, Campbell K, Mishell DR, Grimes DA (1989) Relative frequency of primary ovarian neoplasm: a 10-year review. *Obstet Gynecol* 74:921–926
  68. Outwater EK, Huang AB, Dunton CJ et al (1997) Papillary projections in ovarian neoplasm: appearance on MRI. *J Magn Reson Imaging* 7:689–695
  69. Buy JN, Ghossain MA, Sciote C et al (1991) Epithelial tumors of the ovary: CT findings and correlation with US. *Radiology* 178:811–818
  70. Cho SM, Byun JY, Rha SE et al (2004) CT and MRI findings of cystadenofibromas of the ovary. *Eur Radiol* 14:798–804
  71. Outwater EK, Siegelman ES, Junt JL (2001) Ovarian teratomas: tumor types and imaging characteristics. *Radiographics* 21:475–490
  72. Buy JN, Ghossain MA, Moss AA et al (1989) cystic teratoma of the ovary: CT detection. *Radiology* 171:697–700
  73. Yamashita Y, Hatanaka Y, Torashima M et al (1994) Mature cystic teratomas of the ovary without fat in the cystic cavity: MR features in 12 cases. *AJR Am J Roentgenol* 163:613–616
  74. Caspi B, Appelman Z, Rabinerson D et al (1997) The growth pattern of ovarian dermoid cysts: a prospective study in premenopausal and postmenopausal women. *Fertil Steril* 68:501–505
  75. Rha SE, Byun JY, Jung SE et al (2004) Atypical CT and MRI manifestations of mature ovarian cystic teratomas. *AJR Am J Roentgenol* 183:743–750
  76. Carrington BM (1991) The adnexae. In: Hricak H, Carrington BM (eds) *MRI of the pelvis: a text atlas*. Martin Dunitz, London, pp 185
  77. Togashi K, Nishimura K, Itoh K et al (1987) Ovarian cystic teratomas: MR imaging. *Radiology* 162:669–673
  78. Stevens SK, Hricak H, Campos Z (1993) Teratomas versus cystic hemorrhagic adnexal lesions; differentiation with proton-selective fat-saturation MR imaging. *Radiology* 186:481–488
  79. Brammer HM, Buck JL, Hayes WS et al (1990) Malignant germ cell tumors of the ovary: radiologic-pathologic correlation. *Radiographics* 10:715–724
  80. Heifetz SA, Cushing B, Giller R et al (1989) Immature tera-

- tomas in children: pathologic considerations. *Am J Surg Pathol* 22:1115–1124
81. Kim SH, Kim YJ, Park BK et al (1999) Collision tumors of the ovary associated with teratoma: clues to the correct preoperative diagnosis. *J Comput Assist Tomogr* 23:929–933
82. Matsuki M, Kaji Y, Matsuo M et al (2000) Struma ovarii: MRI findings. *Br J Radiol* 73:87–90
83. Tailor A, Hackett E, Bourne T (1999) Ultrasonography of the ovary. In: Anderson JC (ed) *Gynecologic imaging*. Churchill Livingstone, London, pp 319–343
84. Timmerman D, Moerman P, Vergote I (1995) Meigs syndrome with elevated Ca-125 levels: two case reports and review of the literature. *Gynecol Oncol* 59:405–408
85. Outwater EK, Siegelman ES, Talerman A et al (1997) Ovarian fibromas and cystadenofibromas: MRI features of the fibrous component. *J Magn Reson Imaging* 7:465–71
86. Troiano RN, Lazzarini KM, Scutt LM et al (1997) Fibroma and fibrothecoma of the ovary: MR imaging findings. *Radiology* 204:795–798
87. Moon WJ, Koh BH, Kim SK et al (2000) Brenner tumor of the ovary: CT and MR findings. *J Comput Assist Tomogr* 24:72–76
88. Seidman JD, Russell P, Kurman RJ (2002) Surface epithelial tumors of the ovary. In: Kurman RJ (ed) *Blaustein's pathology of the female genital tract*. Springer Verlag, New York, pp 791–904
89. Matsubayashi R, Matsuo Y, Doi J, Kudo S et al (1999) Sclerosing stromal tumor of the ovary: radiologic findings. *Eur Radiol* 9:1335–1338
90. Yoshitake T, Asayama Y, Yoshimitsu K et al (2005) Bilateral ovarian leiomyomas: CT and MRI features. *Abdom Imaging* 30:117–119
-